LONG-TERM EVOLUTION OF MASSIVE BLACK HOLE BINARIES. III.
BINARY EVOLUTION IN COLLISIONAL NUCLEI

DAVID MERRITT

Department of Physics, 85 Lomb Memorial Drive, Rochester Institute of Technology, Rochester, NY 14623
and
Center for Computational Relativity and Gravitation, School of Mathematical Sciences, 78 Lomb Memorial Drive, Rochester Institute of Technology, Rochester, NY 14623

SEPPO MIKKOLA

Turku University Observatory, Tuorla, 21500 Piikkiö, Finland

ANDRAS SZELL

Department of Physics, 85 Lomb Memorial Drive, Rochester Institute of Technology, Rochester, NY 14623
Draft version February 1, 2008

Abstract

In galactic nuclei with sufficiently short relaxation times, binary supermassive black holes can evolve beyond their stalling radii via continued interaction with stars. We study this "collisional" evolutionary regime using both fully self-consistent N-body integrations and approximate Fokker-Planck models. The N-body integrations employ particle numbers up to 0.26×10^6 and a direct-summation potential solver; close interactions involving the binary are treated using a new implementation of the Mikkola-Aarseth chain regularization algorithm. Even at these large values of N, two-body scattering occurs at high enough rates in the N-body simulations that the binary is never fully in the diffusively-repopulated (i.e. large-N) loss cone regime, which precludes a simple scaling of the results to real galaxies. The Fokker-Planck model is used to bridge this gap; it includes, for the first time in this context, binary-induced changes in the stellar density and potential. The Fokker-Planck model is shown to accurately reproduce the results of the N-body integrations, and is then extended to the much larger N regime of real galaxies. Analytic expressions are derived that accurately reproduce the time dependence of the binary semi-major axis as predicted by the Fokker-Planck model. Gravitational radiation begins to dominate the binary's evolution after a time that is always comparable to, or less than, the relaxation time measured at the binary's gravitational influence radius; the observed correlation of nuclear relaxation time with velocity dispersion implies that coalescence in ≤ 10 Gyr will occur in nuclei with $\sigma \lesssim 80$ km s^{-1}, i.e. with binary black hole mass $\lesssim 2 \times 10^6 M_\odot$. The coalescence time depends only weakly on binary mass ratio. Formation of a core, or "mass deficit," is shown to result from a competition between ejection of stars by the binary and re-supply of depleted orbits via two-body scattering. Mass deficits as large as ~ 4 times the binary mass are produced before the gravitational radiation regime is reached; however, after the two black holes coalesce, a Bahcall-Wolf cusp appears around the single hole in approximately one relaxation time, resulting in a nuclear density profile consisting of a flat core with an inner, compact cluster, similar to what is observed at the centers of low-luminosity elliptical galaxies. We critically evaluate recent claims that binary-star interactions can induce rapid coalescence of binary supermassive black holes even in the absence of loss cone refilling.

Subject headings:

1. INTRODUCTION

This paper is the third in a series investigating the evolution of binary supermassive black holes at the centers of galaxies. A massive binary hardens via exchange of energy and angular momentum with passing stars, but this process is self-limiting, since the interacting stars are ejected from the nucleus with velocities of order the relative velocity of the two black holes. Continued hardening of the binary requires a repopulation of the depleted orbits. Paper I (Milosavljević & Merritt 2003) discussed various mechanisms by which this can occur, including collisional loss-cone repopulation, secondary slingshot, chaotic stellar orbits, and Brownian motion of the binary. These different mechanisms typically obey different scalings of the binary hardening rate with the number N of stars and with time; in the large-N limit and in a spherical or axisymmetric potential, the hardening rate (defined as the rate

of change of the binary's energy) is predicted to scale roughly as N^{-1}, i.e. inversely with the relaxation time, and hence to be very small for values of N characteristic of massive elliptical galaxies (Valtonen 1996; Yu 2002).

In Paper II (Berczik et al. 2005), a direct-summation N-body code, combined with a parallel GRAPE cluster, was used to carry out integrations of binary evolution in galaxy models with large, low-density cores. Because of their low central density, the relaxation time at the center of these models was relatively long (compared with orbital periods), and collisional loss cone refilling was shown to occur at a lower rate than the loss of stars to the binary, i.e. the binary's loss cone remained nearly empty. This is the same ("diffusive") regime believed to characterize binary evolution in real galaxies (Milosavljević & Merritt 2001). The N-body hardening rates were compared with the predictions of simple loss-cone

theory and found to be in reasonable agreement.

The Plummer models used in Paper II were not good representations of real galaxies. In this paper, we present a new set of simulations based on galaxy models that more closely approximate real galaxies, with power-law central density cusps. In order to deal efficiently with interactions involving the binary, we incorporate the Mikkola-Aarseth chain-regularization algorithm (Mikkola & Aarseth 1990, 1993) into our N-body code, including both the effects of nearby stars as perturbers of the chain, and the effects of the chain on the surrounding stars. The resulting N-body algorithm is coupled with a GRAPE-6 special-purpose computer and used to carry out extended integrations of binaries with various values of N, up to the limit $N \approx 0.26 \times 10^6$ set by the GRAPE's memory. In order to more accurately characterize the N-dependence of the evolution, multiple integrations are carried out starting from different random realizations of the same initial conditions and averaged.

Even at the large values of N allowed by the GRAPE-6, two-body (star-star) scattering occurs at a high enough rate in the N-body simulations that the binary is never fully in the empty-loss-cone regime. This fact precludes a simple scaling of the N-body results to real galaxies. We therefore develop a Fokker-Planck model that can be applied to nuclei with any value of N, i.e. any value of $M_{12}/m_\star$, where $M_{12} \equiv M_1 + M_2$ and $m_\star$ are the mass of the binary and of a single star, respectively. Our Fokker-Planck model is unique in that it allows for the joint evolution of the binary and of the stellar nucleus; it can therefore reproduce the creation of a core, or "mass deficit" (Milosavljević et al. 2002), as the binary ejects stars. The Fokker-Planck model is first tested by comparison with the N-body results, and is then applied to the much larger-N regime of real galaxies. In this way we are able to make the first detailed predictions about the joint evolution of massive binaries and stars at the centers of galaxies.

The time scale that limits binary evolution in our models is the relaxation time, defined as the time for (mostly distant) gravitational encounters between stars to establish a locally Maxwellian velocity distribution. Assuming a homogenous and isotropic distribution of equal-mass stars, the relaxation time is approximately

$$T_r \approx \frac{0.34\sigma^3}{G^2 \rho m_\star \ln \Lambda} \qquad (1a)$$

$$\approx 1.2 \times 10^{10} \text{ yr } \sigma_{100}^3 \, \rho_5^{-1} \, \tilde{m}_\star^{-1} \ln \Lambda_{15}^{-1} \qquad (1b)$$

(Spitzer 1987). Here, σ_{100} is the 1d stellar velocity dispersion in units of 100 km s^{-1}, ρ_5 is the stellar mass density in units of $10^5 M_\odot$ pc^{-3}, $\tilde{m}_\star = m_\star/M_\odot$, and $\ln \Lambda_{15} = \ln \Lambda/15$, where $\ln \Lambda$ is the Coulomb logarithm and $\Lambda \approx 0.4N$ (Spitzer 1987).

Figure 1 shows estimates of T_r, measured at the supermassive black hole's influence radius r_h, for the ACS/Virgo sample of early-type galaxies (Côté et al. 2004). The influence radius was defined in the usual way via

$$M_\star(r_h) = 2M_\bullet \qquad (2)$$

and the black hole mass was inferred from the measured value of σ via the the $M_\bullet - \sigma$ relation,

$$M_\bullet \approx 5.72 \times 10^6 M_\odot \sigma_{100}^{4.86} \qquad (3)$$

(Ferrarese & Ford 2005). A stellar mass of $1M_\odot$ was assumed.

Figure 1 reveals a tight correlation between $T_r(r_h)$ and σ. A least-squares fit to the points (shown as the dashed line in the
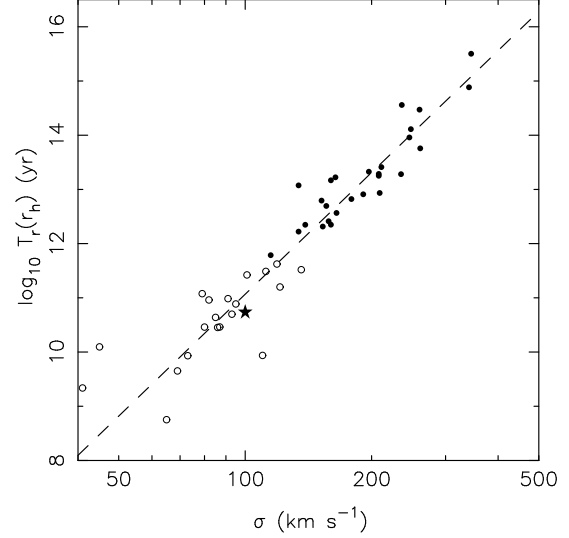

FIG. 1.— Relaxation times, measured at the supermassive black hole's influence radius, in the ACS/Virgo sample of galaxies (Côté et al. 2004), versus the central stellar velocity dispersion. Filled symbols are galaxies in which the black hole's influence radius is resolved; star is the Milky Way.

figure) gives

$$T_r(r_h) \approx 1.16 \times 10^{11} \text{ yr } \sigma_{100}^{7.47} \qquad (4a)$$

$$\approx 8.0 \times 10^9 \text{ yr } M_{\bullet,6}^{1.54} \qquad (4b)$$

where $M_{\bullet,6} \equiv M_\bullet/10^6 M_\odot$. The results presented in this paper are only relevant to galaxies in which the nuclear relaxation time is not much longer than galaxy lifetimes; according to Figure 1, this is the case for galaxies with $\sigma \lesssim 80$ km s^{-1}. This is roughly the velocity dispersion near the center of the Milky Way; hence, the sort of evolution that is modelled here is most relevant to spheroids that are not much brighter than the Milky Way bulge.

The N-body techniques are described in §2 and §3 and the results of the N-body integrations are presented in §4. In §5 the Fokker-Planck model is described and compared with the N-body results. Predictions of the Fokker-Planck model in the large-N regime corresponding to real galaxies are presented in §6. §7 and §8 discuss the implications for evolution of binary supermassive black holes in real galaxies, and §9 presents a critical comparison with other proposed models of binary evolution. §10 sums up.

2. N-BODY TECHNIQUES

Our N-body algorithm was an adaptation of the NBODY1 code of Aarseth (1999) to the GRAPE-6 special purpose hardware. The code uses a fourth-order Hermite integration scheme with individual, adaptive, block time steps (Aarseth 2003). For the majority of the particles, the forces and force derivatives were calculated via a direct-summation scheme using the GRAPE-6. More details of the particle advancement scheme can be found in Paper II. As discussed there, the code contains two parameters that affect the speed and accuracy of the calculation, the particle softening length ε and the time-step accuracy parameter η.

Close encounters between the massive particles ("black holes"), or between black holes and stars, require prohibitively small time steps in such a scheme. To avoid this situation, we adopted a chain regularization algorithm for the critical interactions (Mikkola & Aarseth 1990, 1993), as follows. Let $\mathbf{r}_i$, $i = 1, ..., N$ be the position vectors of the par-

ticles. We first identify the subset of n particles to be included in the chain; the precise criterion for inclusion is presented below, but in the late stages of evolution, the chain always included the two black holes as its lowest members. We then search for the particle that is closest to either end of the chain and add it; this operation is repeated recursively until all n particles are included. Define the separation vectors $\mathbf{R}_i = \mathbf{r}_{i+1} - \mathbf{r}_i$ where $\mathbf{r}_{i+1}$ and $\mathbf{r}_i$ are the coordinates of the two particles making up the ith link of the chain. The canonical momenta $\mathbf{W}_i$ corresponding to the coordinates $\mathbf{R}_i$ are given in terms of the old momenta via the generating function

$$S = \sum_{i=1}^{n-1} \mathbf{W}_i \cdot (\mathbf{r}_{i+1} - \mathbf{r}_i). \qquad (5)$$

Next, we apply KS regularization (Kustaanheimo & Stiefel 1965) to the chain vectors, regularizing only the interactions between neighboring particles in the chain. Let $\mathbf{Q}_i$ and $\mathbf{P}_i$ be the KS transformed $\mathbf{R}_i$ and $\mathbf{W}_i$ coordinates. After applying the time transormation $\delta t = g \delta s$, $g = 1/L$, where L is the Lagrangian of the system ($L = T - U$, where T is the kinetic and U is the potential energy of the system). We obtain the regularized Hamiltonian $\Gamma = g(H(\mathbf{Q}_i, \mathbf{P}_i) - E_0)$, where E_0 is the total energy of the system. The equations of motion are then

$$\mathbf{P}_i' = -\frac{\partial \Gamma}{\partial \mathbf{Q}_i}, \quad \mathbf{Q}_i' = \frac{\partial \Gamma}{\partial \mathbf{P}_i} \qquad (6)$$

where primes denote differentiation with respect to the time coordinate s. Because of the use of regularized coordinates, these equations do not suffer from singularities, as long as care is taken in the construction of the chain.

Since it is impractical to include all N particles in the chain, we must consider the effects of external forces on the chain members. Let $\mathbf{F}_j$ be the perturbing acceleration acting on the jth body of mass m_j. The perturbed system can be written in Hamiltonian form by simply adding the perturbing potential:

$$\delta U = -\sum_{j=1}^{n} m_j \mathbf{r}_j \cdot \mathbf{F}_j(t). \qquad (7)$$

Only one chain was defined at any given time. At the start of the N-body integrations, there was no regularization, and all particles were advanced using the variable-time-step Hermite scheme. The first condition that needed to be met before "turning on" the chain was that one of the particles (including possibly a black hole) achieved a time step shorter than t_{chmin} and passed a distance from one of the black holes smaller than r_{chmin}. If this condition was satisfied, it was then checked whether the encounter resulted in a deflection angle greater than $2\delta = \pi/2$, where

$$\cos \delta = \left[1 + \frac{R^2 V_0^4}{G^2 (m_1 + m_2)^2} \right]^{-1/2}; \qquad (8)$$

here R is the impact parameter, V_0 is the pre-encounter relative velocity, and m_1 and m_2 are the masses of the two particles. This condition is equivalent to

$$m_1 + m_2 > R V_0^2. \qquad (9)$$

Each star closer to the black hole than r_{chmin} was then added to the chain, and the two black holes were always included. The values of t_{chmin} and r_{chmin} were determined by carrying out test runs; we adopted $t_{chmin} \approx 10^{-5} - 10^{-6}$ and $r_{chmin} \approx 10^{-4} - 10^{-3}$ in standard N-body units.
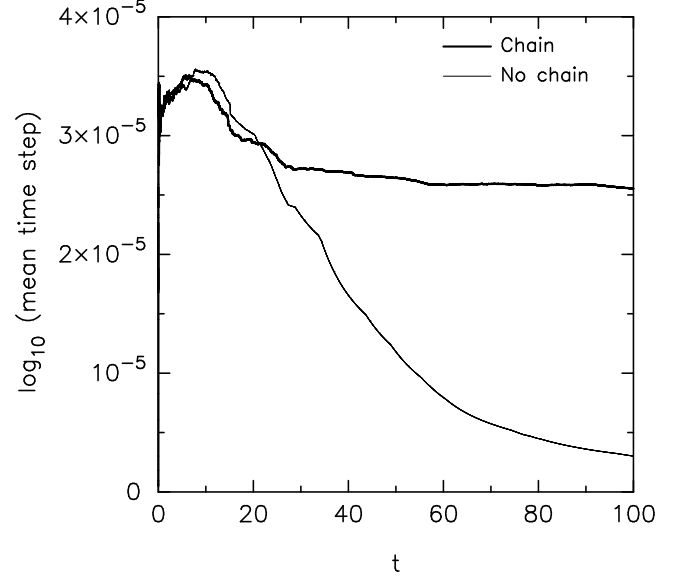

FIG. 2.— The average time step, as defined in the text, during two integrations of a binary black hole at the center of a Dehen-model galaxy. $N = 20,000$, and the softening length and time-step parameters of the N-body code were $\varepsilon = 10^{-6}, \eta = 0.01$. In the absence of the chain, the average time step drops to very low values once the binary begins to harden.
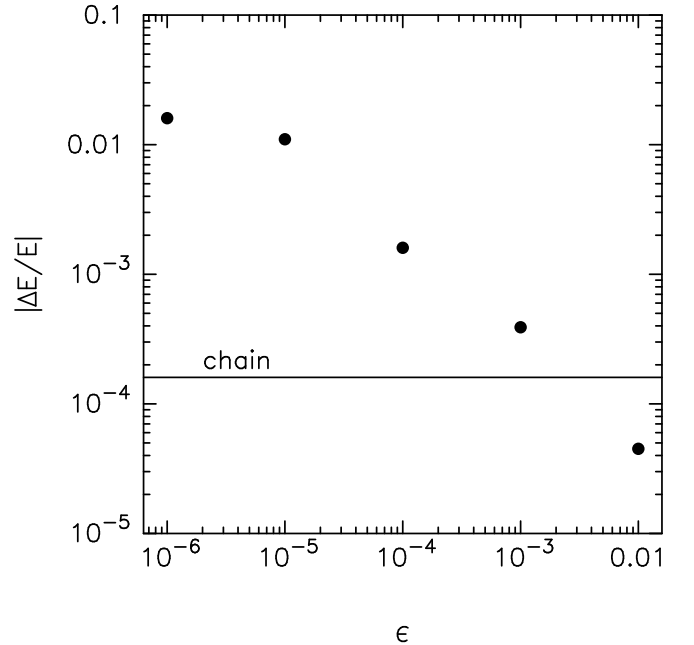

FIG. 3.— Relative energy error over 100 time units of of a set of integrations like those in Fig. 2, for various values of the softening length ε, and with the chain.

The chain's center of mass was a pseudoparticle as seen by the N-body code and was advanced by the Hermite scheme in the same way as an ordinary particle. However, when integrating the trajectories of stars near to the chain, it is essential to resolve the inner structure of the chain. Thus for stars inside a critical r_{crit1} radius around the chain, the forces from the individual chain members were taken into account. The value of r_{crit1} was set by the size of the chain to be $r_{crit1} = \lambda R_{ch}$ with R_{ch} the spatial size of the chain and $\lambda = 100$. In addition, the equations of motion of the chain particles must include the forces exerted by a set of external perturber stars. Whether or not a given star was listed as a perturber was deter-

mined by a tidal criterion: $r < R_{crit2} = (m/m_{chain})^{1/3}\gamma_{min}^{-1/3}R_{ch}$ where m_{chain} represents the mass of the chain, m is the mass of the star, and γ_{min} was chosen to be 10^{-6}; thus $r_{crit2} \approx 10^2 (m/m_{chain})^{1/3}R_{ch}$.

The membership of the chain changed under the evolution of the system. Stars were captured into the chain if their orbits approached the binary closer than R_{ch}. Stars were emitted from the chain if they got further from both of the black holes than $1.5R_{ch}$. The difference between the emission and absorption distances was chosen to avoid a too-frequent variation of the chain membership. When the last particle left the chain, the chain was eliminated and the integration turned back to the Hermite scheme, until a new chain was created.

In what follows, we refer to the N-body code without chain as NB1, and the code including chain as CHNB1. We carried out a number of tests to see how the performance and accuracy of the NB1 code were affected by inclusion of the chain. Typically, one integration step of the chain required about five times as much cpu time as a single call to the GRAPE-6, due to the complex nature of the chain and the generally large number of perturber particles. Thus our code is quicker than a basic Hermite scheme code (NB1) only if the smallest time steps are about an order of magnitude shorter than the next smallest time steps, and if in addition those particles would be assigned to the chain. It is easy to show that in the case of a galaxy including a central, massive binary system this condition is usually fulfilled. The Hermite time step of the binary is considerably smaller than the time steps of the stars, due to their close orbit and fast evolution. Of course, the performance of both codes depends on the two parameters η (time step parameter) and ε (particle softening length) that determine the accuracy of the star-star interactions. In what follows, we fixed $\eta = 0.01$ based on the results of the tests in Paper II. In CHNB1, ε was always set to zero.

Figures 2-4 show the results of our performance tests. Figure 2 plots the average time step as a function of time in both codes, for integrations of a binary black hole in a galaxy model following Dehnen's (1993) density law:

$$\rho(r) = \frac{(3-\gamma)M_{gal}}{4\pi} \frac{a}{r^\gamma(r+a)^{4-\gamma}} \qquad (10)$$

with $\gamma = 1.2$ and $N = 20,000$ particles. The two black holes had equal masses, $M_1 = M_1 = 0.01M_{gal}$, and were placed initially on a circular orbit with separation $0.10a$. We defined the average time step as $t/N_{timesteps}(t)$, where $N_{timesteps}(t)$ was the total number of integration time steps until time t, including only the time steps of particles outside the chain. It can be seen that in the early stages of the evolution, the time steps are about the same in both cases. However as the binary becomes harder, the NB1 time steps become smaller and smaller, in order to achieve the necessary precision in the integration of the binary. In the code with the chain, the average time step hardly changes after the binary begins to harden. The binary is integrated by the regularized equations, hence the step size of the NB1 integration remains relatively large. The average step size of the CHNB1 code was about 2.5×10^{-5} (in units where $G = M_{gal} = a = 1$), while in the NB1 integration it was 3×10^{-6}. The resulting net speed-up with the chain is more than a factor of two.

Figure 3 shows the energy error in a set of integrations of the same model but with various different softening lengths ε, compared with the energy error in an integration with the chain (and $\varepsilon = 0$). It can be seen that the energy conservation
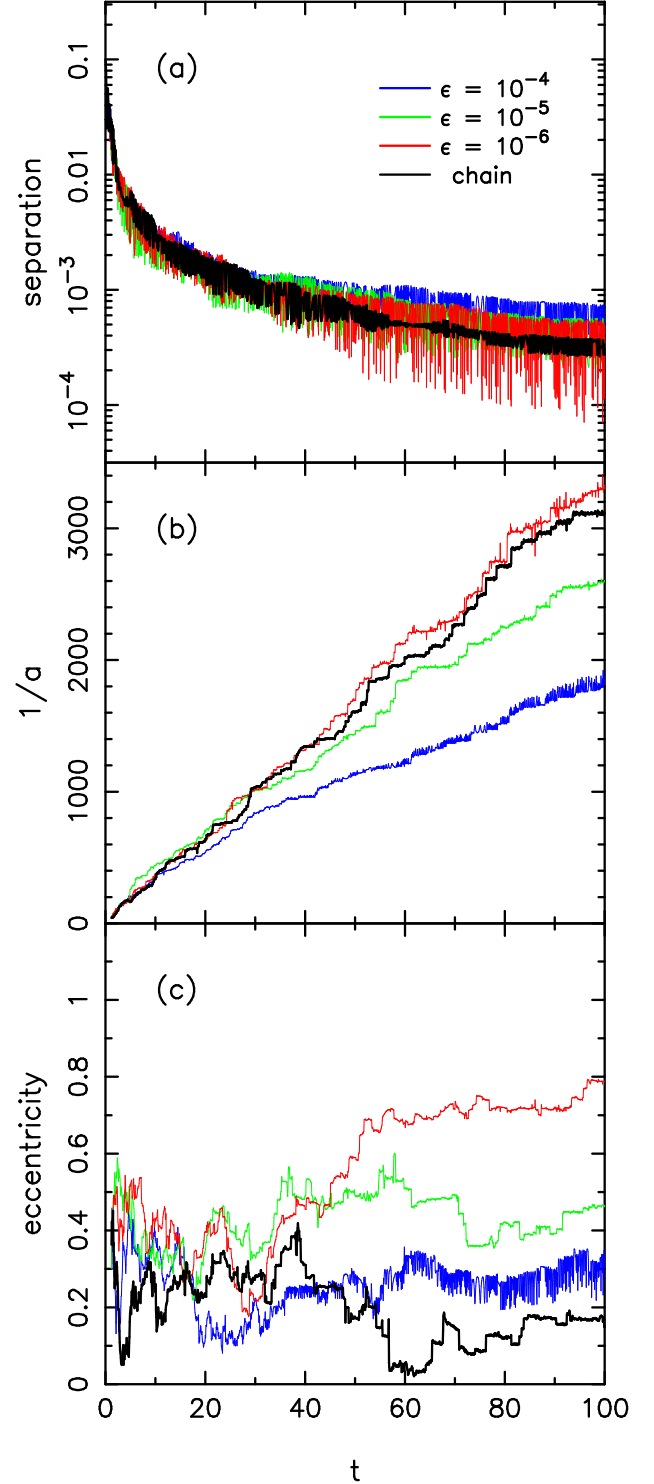

FIG. 4.— Results of a set of test integrations with and without the chain. Initial conditions consisted of a binary of mass $M_1 = M_2 = 0.005$ and separation 0.1, in a Dehnen-model galaxy with $\gamma = 1.2$ and $N = 20,000$.

of the CHNB1 code is about as good as the best results from the NB1 integrations. However, the latter occur when the softening length is very large, much too large for accurate integration of the binary. This is shown in Figure 4. It is evident from that figure that with larger softening lengths, $\varepsilon \gtrsim 10^{-5}$, the integration of the binary is not very accurate. However, even with very small ε, the evolution of the distance between the black holes includes "spiky" behaviors, due apparently to the
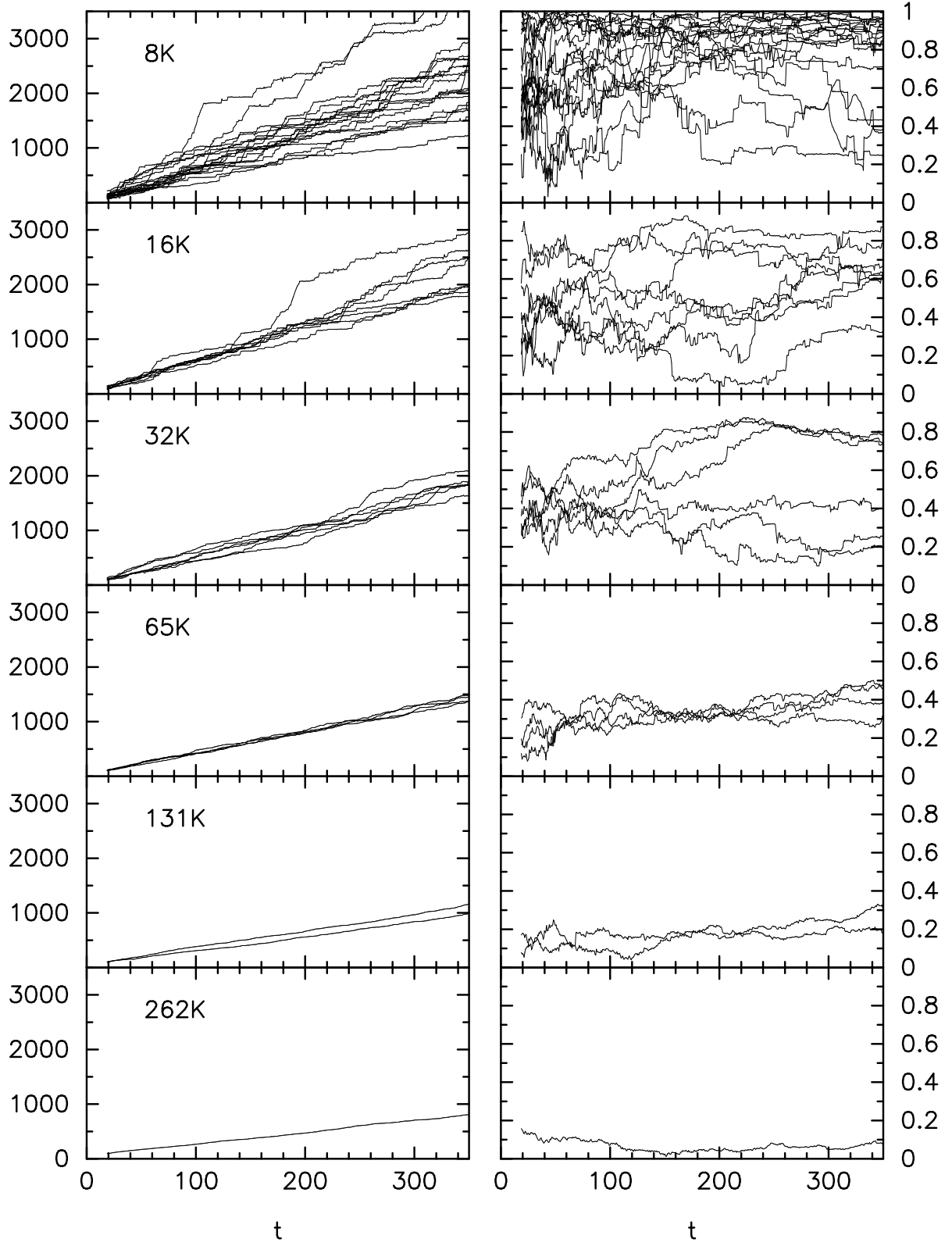
FIG. 5.— Evolution of $1/a$, the inverse binary semi-major axis (left column), and e, the binary eccentricity (right column), in the full set of N-body integrations.

very sensitive nature of the eccentricity evolution with respect to the precision of the integration (Figure 4b,c).

These results suggest that chain regularization is an accurate and efficient way to integrate binary black holes at the centers of galaxies. It can keep track of the evolution of the binary with high precision, and the calculation time is substantially faster than a plain Hermite integration when the latter is used with a reasonable (i.e. sufficiently small) softening parameter.

3. INITIAL CONDITIONS

All of our integrations adopted Dehnen's model, equation (10), for the initial galaxy, with $\gamma = 0.5$. To this model were added two particles, the "black holes," with masses $M_1 = M_2 = 0.005$ in units of the galaxy mass. (Henceforth we write $M_{12} \equiv M_1 + M_2$.) The black holes were placed symmetrically about the center of the galaxy at $x = \pm 0.1$. The initial velocities of the black holes were chosen to be $v_y = \pm 0.16$ yielding nearly circular initial orbits. These initial conditions are similar to those adopted in some earlier studies (Quinlan & Hernquist (1997); Nakano & Makino (1999)) although they are probably less realistic than initial conditions that place one of the two massive particles exactly at the center (e.g. Merritt & Szell (2006)). Henceforth we adopt units such that the gravitational constant G, the total mass in stars M_{gal}, and the Dehnen scale length a are equal to one. In these units, the crossing time $(GM_{gal}/a^3)^{-1/2}$ is also equal to one.

A standard expression for r_h, the radius of influence of a single black hole at the center of a galaxy, is

$$M_\star(r_h) = 2M_\bullet \qquad (11)$$

with $M_\bullet$ the black hole mass and $M_\star(r)$ the mass in stars within a sphere of radius r. The semi-major axis length of a "hard" binary is sometimes defined in terms of r_h as (e.g. Merritt & Wang (2005))

$$a_h = \frac{\alpha}{(1+\alpha)^2} \frac{r_h}{4} \qquad (12)$$

with $\alpha \equiv M_2/M_1 \leq 1$ the binary mass ratio, and we adopt that definition here. Setting $M_\bullet = M_{12} = 0.005 + 0.005 = 0.01$ and $\alpha = 1$, the values of r_h and a_h for our N-body models are

$$r_h = 0.264, \quad a_h = 0.0165. \qquad (13)$$

These expressions ignore the changes that the two black holes induce in the mass distribution of the galaxy when forming a hard binary, but are useful as points of reference.

Based on the results of Papers I and II, once the binary has interacted with and ejected most of the stars on intersecting orbits, its subsequent evolution is dependent on the continued scattering of stars into its sphere of influence; since the scattering time scale increases with N, the binary's decay rate should decrease as N increases. In order to better characterize this N-dependence, the initial conditions were realized using six different values of N, $N = (8192, 16384, 32768, 65536, 131072, 262144)$, or $N = 2^p$, $p = (13, 14, 15, 16, 17, 18)$. (In what follows, we refer to these different N-values via the shorthand 8K, 16K, ..., 262K.) The largest of these N values is close to the maximum number of particles that can be handled in the GRAPE-6 memory. In order to decrease the "noise" associated with the evolution for small N, we carried out n_{int} multiple integrations at each N, in which the initial stellar postions and velocities were calculated using different seeds for the random number generator. All of these integrations were continued until a time $T_{max} = 350$; when scaled to

Name	N	n_{int}
8K	8192	18
16K	16384	8
32K	32768	6
65K	65536	4
131K	131072	2
262K	262140	1

a typical luminous elliptical galaxy with crossing time $\sim 10^8$ yr, this corresponds to $\sim 10^{10}$ yr. Table 1 gives the parameters of the N-body integrations.

4. N-BODY RESULTS

Initially the two black holes move on nearly independent orbits about the center of the galaxy. The orbits decay, and at $t \approx 10$ the black holes form a hard binary. After this, the semimajor axis a of the binary shrinks as the two black holes interact with stars and eject them from the nucleus via the gravitational slingshot. Figure 5 shows the evolution of $1/a$ and e, the orbital eccentricity, in the full set of integrations for $t \geq 20$. The scatter in the values of $1/a$ and e at a given time is considerable in the integrations with smallest N. Nevertheless a clear trend is apparent: both $1/a$ and e evolve less, on average, as N is increased.

4.1. Binary Hardening

In order to clarify the N-dependence of the evolution, we computed averages over the n_{int} independent integrations of $a^{-1}(t)$ and $e(t)$. Figure 6 shows the mean evolution of $1/a$ for the six different N values. The early evolution (Fig. 6a), until $t \approx 10$, is essentially N-independent. In this regime, the hardening of the binary is driven by dynamical friction against the stars, and the rate of binding energy increase is a function only of the stellar density, which is the same for each of the N-body models.

At $t \approx 10$, the binary hardening rate begins to show a clear N-dependence, in the sense of more gradual hardening for larger N. In Merritt (2006), the separation at which this occurs was defined as the "stalling radius," since in the limit of large N the binary would stop evolving at this point. Based on Figure 6, $a_{stall}^{-1} \approx a_h^{-1} \approx 60$ and $t_{stall} \approx 10$.

At $t \gtrsim t_{stall}$ the N-dependence of the evolution is striking (Fig. 6b). As in Paper II, we define the instantaneous hardening rate as

$$s(t) \equiv \frac{d}{dt}\left(\frac{1}{a}\right). \qquad (14)$$

Figure 7 shows $\langle s \rangle(t)$ computed by fitting smoothing splines to the averaged $a^{-1}(t)$ curves of Figure 6b. Mean hardening rates are roughly constant with time for each N. The N-dependence of the hardening rate is shown in Figure 8. Here, $\langle s \rangle$ was computed by fitting a straight line to $\langle a^{-1} \rangle(t)$ in an interval $\Delta t = 50$ centered on $\langle a^{-1} \rangle(r) = 750$; in this way, the different hardening rates are being compared at similar values of the binary semi-major axis, chosen to be roughly the minimum value reached in the integration with largest N. The dependence of $\langle s \rangle$ on N is approximately a power law,

$$\log_{10} \bar{s} \approx 2.27 - 0.357 \log_{10} N. \qquad (15)$$

The $\sim N^{-0.4}$ dependence is considerably flatter than the $\sim N^{-1}$ dependence expected in a diffusively-refilled loss cone
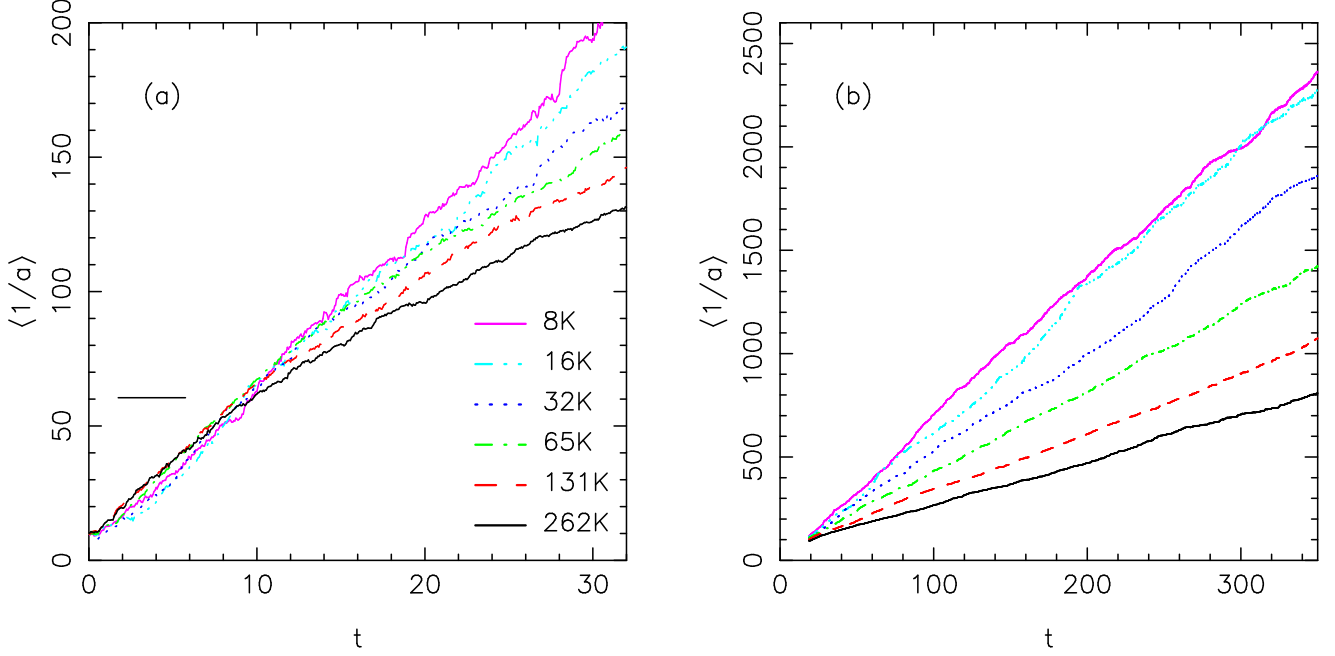
FIG. 6.— Short-term (a) and long-term (b) evolution of the mean value of $1/a$ in the N-body integrations. Horizontal line in panel (a) indicates approximately where the transition occurs between N-independent and N-dependent evolution; this is also roughly the "stalling radius" defined in Merritt (2006), and the "hard binary" separation defined in Yu (2002).

(Milosavljević & Merritt 2003). This fact precludes any simple extrapolation of the data in Figure 8 to the much larger N regime of real galaxies.

We can compare these hardening rates with the predictions of scattering experiments in a fixed, infinite, homogeneous background:

$$s \equiv \frac{d}{dt}\left(\frac{1}{a}\right) = H\frac{G\rho}{\sigma} \qquad (16)$$

with ρ and σ the mass density and 1d velocity dispersion of the stars, and H a dimensionless rate coefficient that depends on the binary separation, mass ratio and eccentricity. For a hard, equal-mass, circular-orbit binary, $H \approx 16$ (Hills 1983; Mikkola & Valtonen 1992; Quinlan 1996a; Merritt 2001). Unfortunately, neither ρ nor σ are well defined for our N-body models: ρ is formally divergent as $r \to 0$ (eq. 10), and σ drops to zero at the origin in the absence of the central binary (Dehnen 1993). We can crudely evaluate equation (16) by setting $\rho \approx 0.595(0.338)$ and $\sigma \approx 0.216(0.244)$, the mean and mass-weighted, rms values within a sphere of radius $0.1(0.2)$ about the center of the (binary-free) Dehnen model. The results, with $H = 16$, are $s \approx 44(22)$. These are likely to be overestimates: the central density of the galaxy drops as the binary ejects stars and the central velocity dispersion is increased by the presence of the binary. If we decrease ρ by a factor of two to account for ejections and set σ equal to the rms velocity dispersion in the $\gamma = 0.5$ Dehnen model containing a central, $M = 0.01$ point mass, the predicted hardening rates drop to $\sim 13(8)$. These numbers are reasonably consistent with the low-N hardening rates shown in in Figure 8, $\bar{s} \approx 6.5$, suggesting that the binary is approximately in the "full loss cone" regime at these low values of N.

4.2. Eccentricity Changes

The N-dependence of the eccentricity evolution (Figure 9) is not quite so transparent. Although the two black holes were initially placed on circular trajectories, perturbations from passing stars sometimes resulted in very non-zero ec-
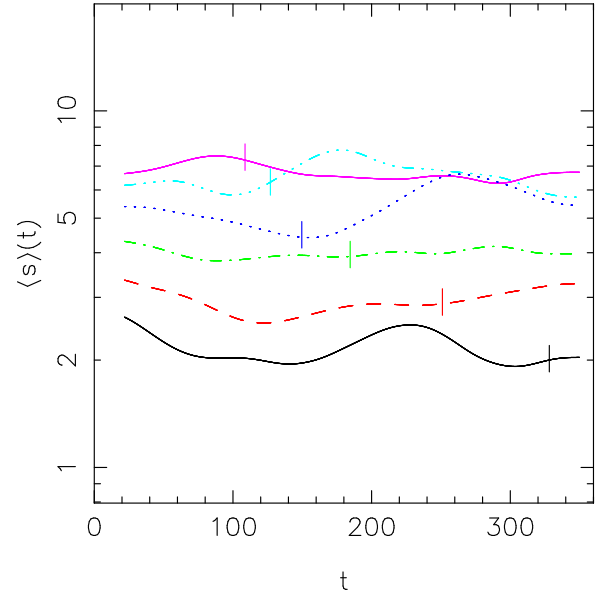

FIG. 7.— Binary hardening rate as a function of time, computed as an average over the n_{int} independent integrations at each N. Line styles have the same meaning as in Figure 6. Tick marks indicate where the hardening rate was evaluated for Fig. 8, i.e., at $\langle a^{-1} \rangle = 750$.

centricities developing around or even before the time the binary became hard. This was especially true in the small-N integrations (Fig. 5); for $N = 8K$, the mass ratio between black hole and star was only 40 and a single star-binary interaction at early times could induce a substantial change in the binary's orbit. Once established at early times, these eccentricities tended to persist. Spurious changes in e in small-N-body simulations have been noted by other authors (Quinlan & Hernquist 1997; Milosavljević & Merritt 2001). However the general trend in Figures 5 and 9 is clearly toward smaller eccentricities for larger N.

Statements about eccentricity evolution of massive binaries are often based on the results of three-body scattering ex-
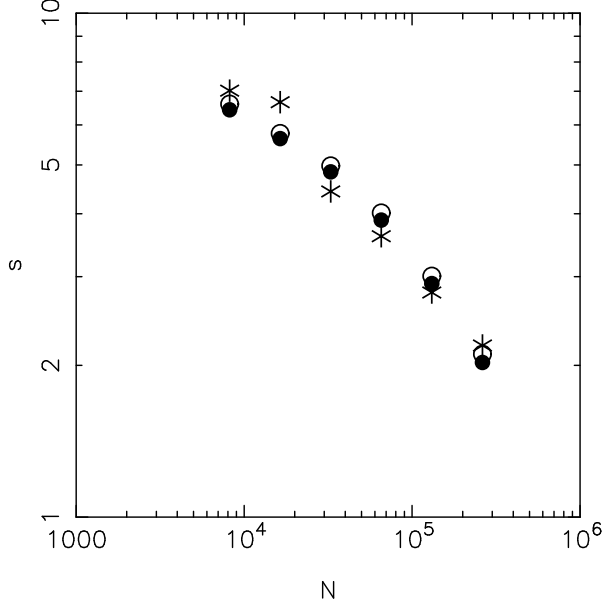
FIG. 8.— N-dependence of the binary hardening rate, computed by fitting $a^{-1}(t)$ in an interval $\Delta t = 50$ centered on $a^{-1} = 700$. *Asterices*: N-body results (Fig. 6(b)), computed as averages over the set of ensembles at each N. *Filled circles*: Fokker-Planck results (Fig. 14), omitting the "secondary slingshot." *Open circles*: Fokker-Planck results, including the "secondary slingshot."

periments (Mikkola & Valtonen 1992; Quinlan 1996a; Merritt 2001). In these experiments, changes in e are typically expressed in terms of changes in a as

$$\left\langle \frac{de}{dt} \right\rangle = K \left\langle \frac{d}{dt} \ln \left(\frac{1}{a} \right) \right\rangle \qquad (17)$$

where $K = K(e,a)$ is a dimensionless rate coefficient and $\langle \rangle$ indicates averages over impact parameter and velocity at infinity. Mikkola & Valtonen (1992) and Quinlan (1996) give approximate analytic fits to $K_1(e,a,v_\infty)$, the impact-parameter-averaged rate coefficient describing changes in e due to interaction of the binary with stars of a *single* velocity v_∞. These expressions for K_1 can be converted into expressions for K by averaging over an assumed velocity distribution at infinity, and Quinlan (1996, Fig. 9) shows the results of such a calculation. (Sesana et al. 2006 present similar plots.) Evolution is always found to be in the direction of increasing eccentricity, i.e. $K \geq 0$, excepting possibly in the case of soft, nearly-circular binaries (Quinlan 1996, Fig. 9d-f). Evolution rates tend to increase with increasing hardness of the binary, reaching maximum values of $K \approx 0.2$ for equal-mass binaries with $e \approx 0.75$ and falling to zero at $e = 0$ and $e = 1$. This is at least qualitatively consistent with Figure 9, which shows $de/d\ln(1/a)$ generally increasing at late times, i.e. for larger binding energies.

Comparing these predictions quantitatively with the N-body experiments is desirable, but problematic for a variety of reasons, the most important of which is probably the strong dependence of K on σ/V_{bin}, where σ is the stellar velocity dispersion (assumed independent of position) and V_{bin} the binary orbital velocity. In galaxy models like ours, σ is a steep function of radius near the galaxy's center and it is not clear what value to choose.

In the limit of large binding energy, $V_{bin} \gg \sigma$, the velocity at infinity is irrelevant and K as determined by the scattering experiments becomes independent of a. Mikkola & Valtonen
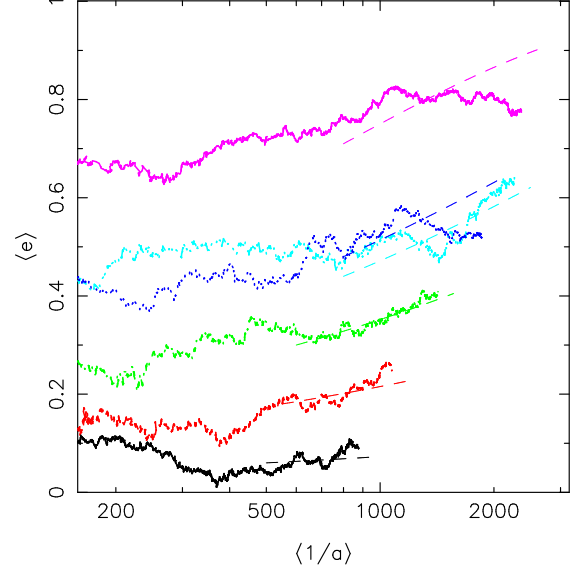

FIG. 9.— Evolution of the mean value of e. Each line is an average of the e values in the various N-body integrations that started from different random realizations of the same initial conditions. Dashed lines show solutions to equation (20).

(1992) find for K in this limit the approximate expression

$$K(e) \approx \frac{(1-e^2)}{2e} \left[(1-e^2)^m - 1 \right], \qquad (18a)$$

$$m = 0.3e^2 - 0.8 \qquad (18b)$$

while Quinlan (1996) gives, for an equal-mass binary in the large-binding-energy limit,

$$K(e) \approx e \left(1-e^2 \right)^{k_0} (k_1 + k_2 e), \qquad (19a)$$

$$(k_1, k_2, k_3) = (0.731, 0.265, 0.230). \qquad (19b)$$

Figure 10 shows that the two expressions are in good agreement.

A rough value of σ/V_{bin} in our simulations is $\sim 2a^{1/2}$, where σ has been set to ~ 0.2, its mean value within a sphere of radius 0.1 (neglecting the effects of the binary). For a^{-1} in the range $500 \lesssim a^{-1} \lesssim 2500$ (Fig. 6), this expression gives $0.1 \gtrsim \sigma/V_{bin} \gtrsim 0.04$. Figure 9 from Quinlan (1996) suggests that $K(e)$ reaches its large-binding-energy limit for $\sigma/V_{bin} \lesssim 0.05$, so our simulations should be in or near this regime at late times.

Accordingly, Figure 9 shows solutions to

$$de = K(e) \, d\ln a^{-1} \qquad (20)$$

using Quinlan's expression for $K(e)$. The agreement with the N-body results is quite reasonable, especially for the larger values of N. Nevertheless, we stress again that the final eccentricity values in our N-body simulations are influenced strongly by noise-induced changes in e at early times, and these changes would be much smaller in the large-N regime of real galaxies.

4.3. *Mass Deficits*

As the binary hardens, it ejects stars from the nucleus and lowers its density. These density changes are sometimes estimated from scattering experiments in a fixed background like those described above, e.g. the change in core mass
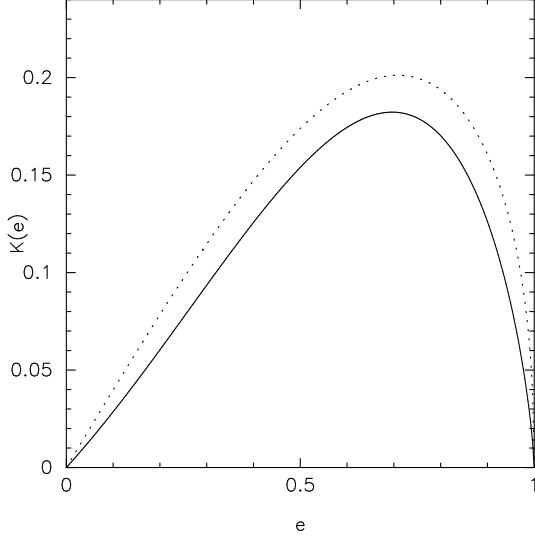
FIG. 10.— Two approximations, derived from three-body scattering experiments, for the coefficient K (eq. 17) describing the rate of eccentricity evolution in the limit of large binding energy. *Solid line:* Quinlan (1996); *dashed line:* Mikkola & Valtonen (1992). The solid line was used to computed the evolutionary tracks (dashed lines) in Fig. 9.

is equated with the mass "ejected" by the binary. However the fact that the binary continues to harden at late times (Fig. 6b) implies that depopulated orbits are continually being re-supplied. Changes in nuclear density are therefore a competition between ejection of stars (some of which may remain bound to the core) and re-population of orbits by gravitational scattering. A number of other mechanisms can also influence the evolution of the central density; for instance, loss of matter from the core lowers its binding energy and causes it to expand. The net effect of these various processes is difficult to estimate without full N-body simulations.

We follow the standard practice of describing changes in core mass in terms of the mass deficit M_{def}, defined by Milosavljević et al. (2002) as the difference in integrated mass between the density profile and the initial density profile, within the region influenced by the binary. Mass deficits have been estimated in a number galaxies (Milosavljević et al. 2002; Ravindranath et al. 2002; Graham 2004; Merritt 2006) using assumed forms for the pre-existing density profile. Figure 11 shows M_{def} versus time, and versus binary semi-major axis, for the averaged N-body integrations.

As in previous work (Milosavljević & Merritt 2001; Merritt 2006), we find that the mass deficit increases suddenly when $a \approx a_h$, to a value $M_{def} \approx M_{12}$. Since the initial conditions adopted here are rather artificial – neither of the black hole particles was placed at the center, for instance – the value which we find for M_{def} at this time may not accurately reflect the value following a real galaxy merger. We therefore present in Figure 11 $M_{def} - M_{def,h}$, the *change* in the mass deficit since the time at which $a = a_h$; as above, we take this time to be $t = 10$ (Fig. 6).

When plotted vs. a_h/a (Fig. 11b), the N-dependence of the evolution almost disappears, allowing the differential mass deficit to be expressed almost uniquely in terms of the change in semi-major axis. As shown below, a binary would not be expected to evolve past $a^{-1} \approx 100a_h^{-1}$ before gravitational wave losses begin to dominate the evolution, implying a maximum mass deficit of $\sim 5M_{12}$; however an extrapolation of this prediction to the much larger N regime of real galaxies would be dangerous. Figure 12 shows averaged density profiles at

various times for the integrations with $N = 65K$.

5. THE FOKKER-PLANCK MODEL

As shown in Figure 8, the N-dependence of binary hardening rate in the N-body simulations is $s \sim N^{-0.4}$. This is substantially flatter than the $\sim N^{-1}$ dependence expected in a diffusively-repopulated ("empty") loss cone (Milosavljević & Merritt 2003), which makes it difficult to extrapolate the N-body results to the regime of real galaxies. In this section we develop a Fokker-Planck model that can reproduce the N-body results and which can also be applied to systems with arbitrarily large N. Unlike previous treatments of this problem based on encounter theory, we allow the radial distribution of matter to evolve in our Fokker-Planck models, due both to loss of stars that interact with the binary, and to diffusion in energy of non-interacting stars. These improvements will be shown to be crucial for accurately reproducing the N-body results. They also allow us, for the first time, to make quantitative predictions about the evolution of the mass deficit in galaxies where binary evolution is driven by collisional loss-cone repopulation.

5.1. *Loss-cone Dynamics*

Consider a spherical galaxy containing a massive central binary that acts like a sink, ejecting stars that come sufficiently close to it. Let $E = -v^2/2 + \psi(r)$ be the binding energy per unit mass of a star in the combined potential $\Phi(r) = -\Psi(r)$ of the galaxy and the binary; the latter is approximated as $-GM_{12}/r$. The binary defines a loss cone of orbits that satisfy $J \lesssim J_{lc}(E)$, where

$$J_{lc}^2(E) = 2r_{lc}^2 [\psi(r_{lc}) - E] \approx 2GM_{12}r_{lc}; \qquad (21)$$

here J is the angular momentum per unit mass of a star and r_{lc} is the radius of the ejection sphere around the binary.

Suppose that the binary has interacted with and ejected all stars that were initially on orbits satisfying $J \leq J_{lc}$. (In Fig. 6, this appears to have occurred by a time of ~ 15.) The binary's subsequent hardening is limited by the rate at which stars are scattered onto previously depleted loss-cone orbits. A fundamental quantity is the ratio $q_{lc}(E)$ between the orbital period $P(E)$ and the (orbit-averaged) time scale for diffusional refilling of the consumption zone (Paper I):

$$q_{lc}(E) \equiv \frac{1}{R_{lc}(E)} \oint \frac{dr}{v_r} \lim_{R \to 0} \frac{\langle (\Delta R)^2 \rangle}{2R}. \qquad (22)$$

Here $R \equiv J^2/J_c(E)^2$ is a dimensionless angular momentum variable, $0 \leq R \leq 1$, with $J_c(E)$ the angular momentum of a circular orbit of energy E, and $\langle (\Delta R)^2 \rangle$ is the diffusion coefficient associated with R. The limit $R \to 0$ in equation (22) reflects the approximation that only very eccentric orbits are scattered into the binary; the orbital period is likewise defined in terms of a $J = 0$ orbit. This approximation breaks down for the most bound orbits but as we show, almost all of the loss cone repopulation comes from stars weakly bound to the binary.

In the case of orbits with periods much shorter than the refilling time ($q_{lc} \ll 1$), the system is "diffusive" and the loss cone is largely empty. For orbits with periods much longer than the refilling time ($q_{lc} \gg 1$), the system is in the "pinhole" or "full loss cone" regime. In a galaxy containing a binary with fixed r_{lc}, q_{lc} increases with decreasing E, i.e. with increasing distance from the binary. The energy at which $q_{lc} = 1$ is defined as the critical energy, E_{crit}, that separates
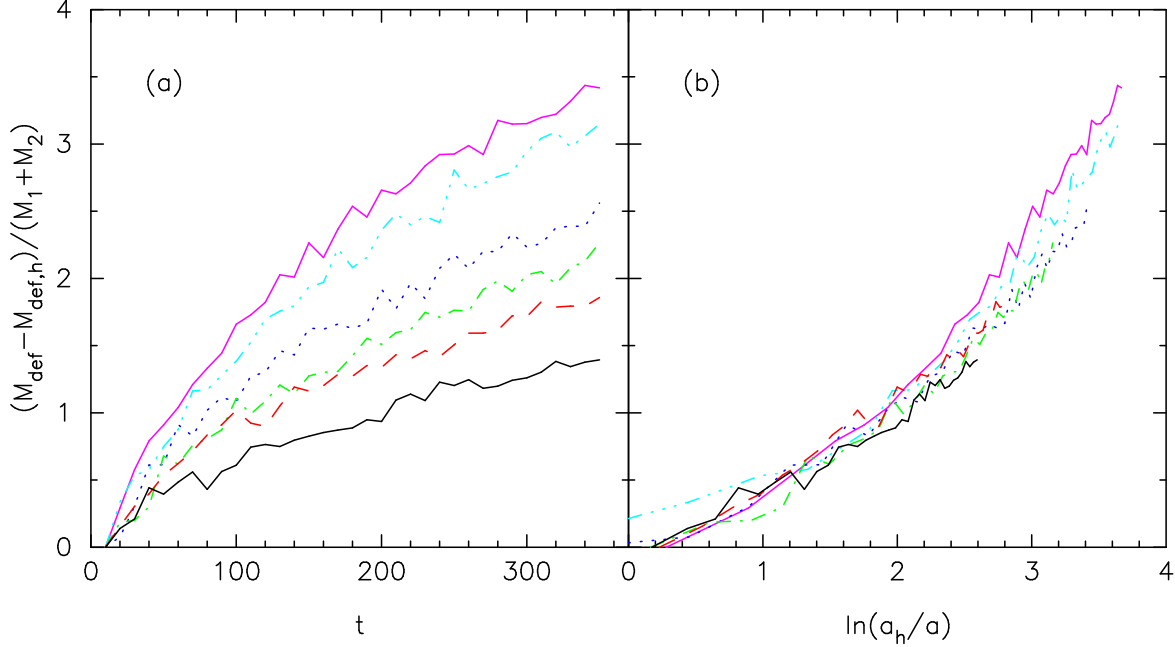
FIG. 11.— Evolution of the mass deficits in the N-body integrations, vs. time (a) and semi-major axis (b). a_h is the binary separation at $t = 10$, when the hard binary forms, and $M_{def,h}$ is the mass deficit at this time. Line styles have the same meaning as in Figure 6.
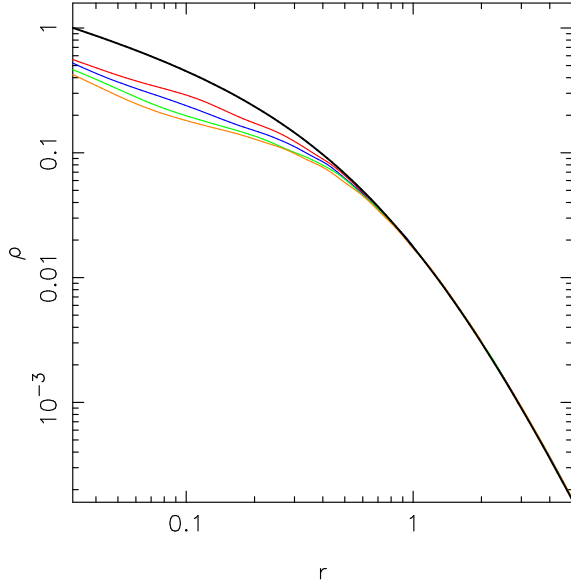

FIG. 12.— Evolution of the mean density profile in the 64K integrations. Black: $t = 0$; red: $t = 50$; blue: $t = 150$; green: $t = 250$; orange: $t = 350$.

empty- from full loss cone regimes. The N-dependence of the problem appears via the angular momentum diffusion coefficient $\langle (\Delta R^2) \rangle$, which scales (approximately) linearly with the mean stellar mass, i.e. inversely with N for a fixed mass of the galaxy (Paper I). Other factors that influence q_{lc} are the degree of central concentration of the galaxy (high central density implies larger q_{lc}) and the size r_{lc} of the interaction sphere (i.e. the binary semi-major axis). Milosavljevic & Merritt (2003) show that massive binaries in real galaxies ($N \gtrsim 10^9$) are essentially always in the empty loss cone regime, even in the extreme case of a $\rho \sim r^{-2}$ stellar density cusp, due to the long relaxation times and to the large physical size of a binary.

As a first step toward understanding the evolution of the binary in our N-body simulations, we plot in Figure 13a $q_{lc}(E)$ for our initial galaxy model, assuming two values for r_{lc} at

each N: $r_{lc}^{-1} = 100$, corresponding to the time $t \approx 15$ when the hardening rate has just begun to exhibit a dependence on N (Fig. 6); and $r_{lc} = a(t = 350)$, the final value of a (different for each N). This figure suggests that none of the integrations was fully in the empty loss cone regime characteristic of real galaxies; even for $N = 262k$, $q_{lc} > 1$ except at energies close to $\psi(r_h)$ (as defined above, r_h is the gravitational influence radius of the central mass, i.e. the radius containing a mass in stars equal to twice M_{12}). As the binary hardens, q_{lc} increases in all of the simulations, and at the final time step, $q_{lc} > 1$ at $E < \psi(r_h)$ for all N, i.e. the binary has evolved essentially completely into the full loss cone regime.

A more useful characterization of the binary's loss cone is shown in Figure 13b. For this figure, the flux of stars into r_{lc} was computed, and broken into two parts: the flux F_{full} originating from stars at energies such that $q_{lc} \geq 1$; and F_{empty}, from stars with energies such that $q_{lc} < 1$. The energy-dependent flux $\mathcal{F}(E)$ can be derived from the orbit-averaged equation describing diffusion in J (Eq. 19, Paper I):

$$\frac{\partial \mathcal{N}}{\partial t} = \frac{R_{lc}}{P} q_{lc} \frac{\partial}{\partial R} \left(R \frac{\partial \mathcal{N}}{\partial R} \right), \qquad (23)$$

where $\mathcal{N}(E, R, t) = 4\pi^2 P(E) J_c^2(E) f(E, R, t)$ is the number density of stars in the (E, R) plane. [1] The flux into the bi-

---

[1] We assume in writing equation (23) that the orbit-averaged Fokker-Planck equation can be applied near the loss-cone boundary. This is valid for the diffusively-repopulated loss cone of a binary in a real galaxy, but may not be valid at low energies in the N-body simulations since the loss cone is nearly full and the separation of time scales on which the orbit-averaging is based breaks down. Nevertheless equation (23) is traditionally applied even in this regime (Cohn & Kulsrud 1978; Magorrian & Tremaine 1999). Our expression for the flux does tend to the correct limit in the full loss cone regime, $q_{lc} \gg 1$. See Shapiro & Marchant (1982) for a treatment of the loss cone that is not based on the orbit-averaged approximation
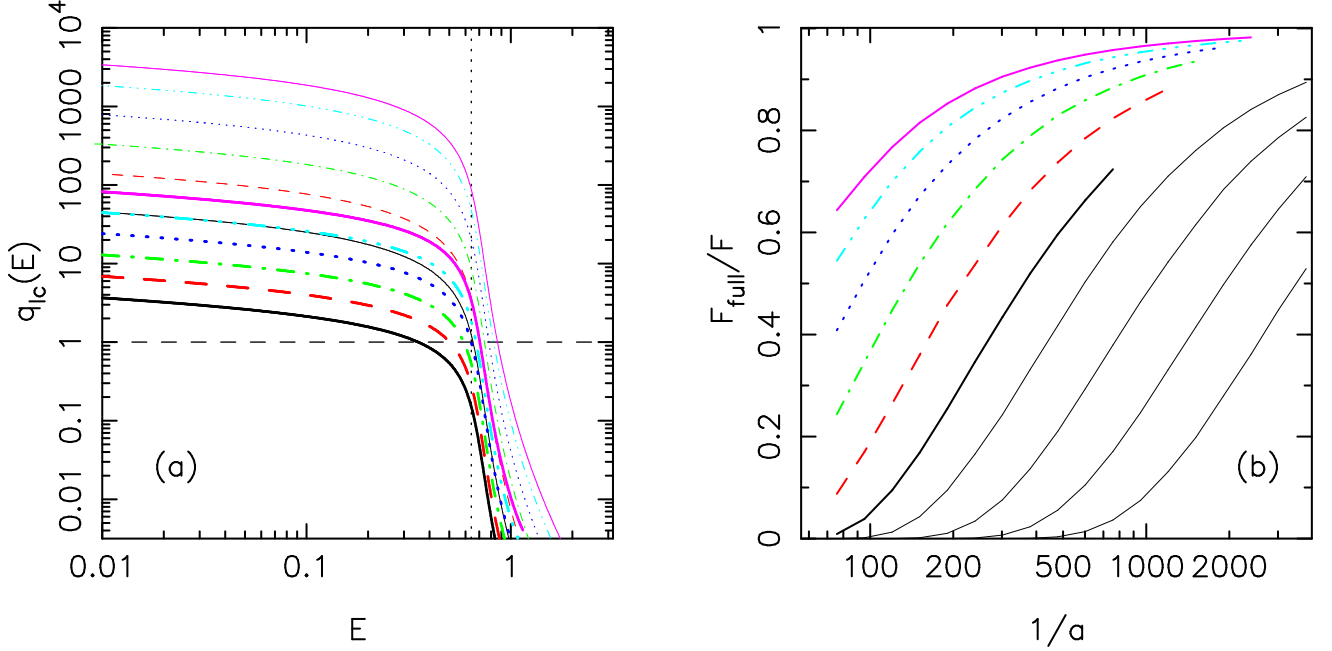
FIG. 13.— (a) The function $q_{lc}(E)$ that describes the ratio of the orbital period at E to the timescale for diffusional refilling of the loss cone; $q \gg 1$ indicates that the loss cone is "full," and real galaxies have $q_{lc} < 1$. Line styles have the same meaning as in Figure 6. Thick curves show q_{lc} for $a^{-1} = 100$, when binary has just entered the N-dependent phase of its evolution (Fig. 6). Thin curves show q_{lc} for the binary at the final time step, $t = 350$; the binary separation at this time is different for each N. The radius of the loss sphere has been set to a. Vertical dotted line is $E = \psi(r_h)$. (b) The fraction of the flux of stars into the binary's loss cone that is contributed at energies where $q_{lc} \geq 1$, i.e., where the loss cone is essentially full. Lines show predictions for $N = (0.5, 1, 2, 4) \times 10^6$. These plots ignore binary-induced changes in the mass distribution of the galaxy.

nary is

$$\mathcal{F}(E)dE = \left[-\frac{d}{dt} \int_{R_0}^1 \mathcal{N}(E,R,t)dR \right] dE \quad (24a)$$

$$= -\frac{R_{lc}}{P} q_{lc} \left[R\frac{d\mathcal{N}}{dR} \right]_{R_0}^1 dE \quad (24b)$$

$$= 4\pi^2 J_{lc}^2(E) q_{lc}(E) \left[R\frac{\partial f}{\partial R} \right]_{R_0} dE. \quad (24c)$$

In these expressions, f has been allowed to fall to zero at an angular momentum $R_0(E)$ that is different from $R_{lc}(E)$. Cohn & Kulsrud (1979) derived an approximate expression for R_0:

$$R_0(E) = R_{lc}(E) \times \begin{cases} \exp(-q_{lc}), & q_{lc}(E) > 1 \\ \exp(-0.186q_{lc} - 0.824\sqrt{q}), & q_{lc}(E) < 1. \end{cases}$$

For $q_{lc} \ll 1$, $R_0 \approx R_{lc}$ but as q_{lc} increases, the loss cone is largely full and $R_0 \approx 0$. Finally, we adopt the steady-state solution to equation (23) for f, i.e.

$$f(R;E) = \frac{\ln(R/R_0)}{\ln(1/R_0) - 1} \overline{f}(E) \quad (25)$$

(assuming $R_0 \ll 1$) implying a diffusive flux

$$\mathcal{F}(E)dE = 4\pi^2 J_{lc}^2(E) q_{lc}(E) \frac{\overline{f}(E)}{\ln(1/R_0) - 1} dE. \quad (26)$$

Here, $\overline{f} = \int_0^1 f(E,R)dR$ is the isotropic f that has the same total number of stars at each E as the true $f(E,R)$.

As noted above, the loss cone of a binary black hole in a real galaxy is essentially empty, i.e. almost all of the stars scattered into the binary would come from energies $E > E_{crit}$. Figure 13b shows the results of applying equation (26) to our initial N-body model, with $r_{lc} = a$ and with a allowed to vary over the range $100 \leq a^{-1} \leq a_{t=350}^{-1}$. In this figure, F_{full} is

the flux integrated from 0 to E_{crit} and F is the total flux. At the start of the N-body integrations, Figure 13b suggests that the binary in the larger-N models ($N \gtrsim 64k$) is essentially in the empty loss cone regime, $F_{full} \ll F$. However by the final time step, the binary has shrunk and entered into the "pinhole" regime, $F_{full} > F_{empty}$, for all N. In the integrations with $N \lesssim 16k$, the binary is in the full loss cone regime from the start.

Figure 13b also includes curves for the cases $N = (0.5, 1, 2, 4) \times 10^6$. Values of N up to 4×10^6 are now computationally feasible via direct-summation codes combined with special-purpose hardware (Harfst et al. 2006), and Figure 13b suggests that this N value is large enough to place the binary effectively in the empty loss cone regime for most of its evolution. (The minimum required N would be larger than this if the binary were given the smaller mass, $\sim 10^{-3} M_{gal}$, typical of black holes in real galaxies, or if the galaxy model were more centrally concentrated.)

Figure 13 illustrates the difficulty of scaling the binary evolution observed in our N-body simulations to real galaxies. In the empty loss cone (i.e. diffusive, large-N) limit, the supply of stars to the binary scales as $\langle (\Delta R^2) \rangle \propto m_\star \propto N^{-1}$ for a fixed total galaxy mass (ignoring the weak dependence of the Coulomb logarithm on N). In the full loss cone (pinhole, small-N) limit, the loss cone flux is independent of N. In between these limiting cases, one expects (Paper I) that the flux, and hence the hardening rate of the binary, scales as $\sim N^{-\beta}$, $0 < \beta < 1$. This is consistent with the $s \sim N^{-0.36}$ dependence observed here (equation 15). Figure 13b suggests that of order $N \approx 10^7$ stars would be required before the binary is comfortably in the empty loss cone regime, allowing its evolution to be reliably scaled to larger values of N.

Even if we were in this regime, the expressions given above for the flux of stars into the binary's loss cone might not accurately predict the binary's evolution, since they ignore

changes in the galaxy's structure. Figure 12 suggest that these changes are significant: the density near the galaxy's center changes by a factor ~ 2 as the binary hardens. We now consider a model that includes both changes in the binary due to interaction with stars, as well as binary-induced changes in the stellar distribution, and that can be reliably scaled to the large-N regime of real galaxies.

5.2. *Evolutionary Model*

The J-directed flux of stars into the binary, described by equation (26), implies a decrease in the number of stars at $J_{lc} \lesssim J \lesssim J_c(E)$. In Paper I, this decrease was followed by integrating equation (23) forward in time at fixed E. The justification for treating the problem in this restricted way was the difference in time scales between E- and J-diffusion; the former occurs in a time $\sim T_r$ while the latter requires $\sim (a_h/r)T_r$. The evolution of $f(J;E)$ and $\mathcal{F}(E)$ over the shorter of these time scales was followed starting from a completely emptied loss cone and the change in the density of the core was computed from the changes in $N(J;E)$ at every E.

In the present paper, we focus on changes that take place over the longer of these two time scales, $\sim T_r$. This allows us to largely ignore the initial conditions, and to assume that an expression like (25) is an adequate description of the J-dependence of f at every E. However it also implies that we can not ignore changes in E, which occur on timescales of $\sim T_r$.

On these longer time scales, the evolution of the density near the binary is a competition between loss of stars that diffuse onto low-J orbits and are ejected by the binary, as described by $\mathcal{F}(E)$, and replenishment due to stars that diffuse in energy from regions of lower E, i.e. larger radius. Beyond a certain radius, the relaxation time is so long that the E-directed flux can not compensate for the integrated loss-cone flux, $\int \mathcal{F}(E)dE$, and the mean density within this radius must drop – implying the creation of a mass deficit.

We can approximate the evolution of the galaxy/binary system in this late-time regime via a modification of the orbit-averaged Fokker-Planck equation for $f(E)$:

$$\frac{\partial N}{\partial t} = -\frac{\partial F_E}{\partial E} - \mathcal{F}(E,t), \qquad (27)$$

where $\mathcal{F}$ is the J-directed flux defined in equation (26), and F_E is the energy-directed flux, given by

$$F_E = -D_{EE}\frac{\partial f}{\partial E} - D_E f \qquad (28a)$$

$$D_{EE} = 64\pi^4 G^2 m_\star \ln\Lambda \left[q(E)\int_0^E dE' f(E') \right.$$

$$\left. + \int_E^\infty dE' q(E') f(E') \right], \qquad (28b)$$

$$D_E = -64\pi^4 G^2 m_\star \ln\Lambda \int_E^\infty dE' p(E') f(E') \qquad (28c)$$

In these expressions, $f(E)$ is understood to be the *mass* density of stars in phase space associated with the function $\overline{f}(E)$ defined above, and the quantities F_E and $\mathcal{F}$ are mass fluxes. $N(E)dE = 4\pi^2 p(E)f(E)dE$ is energy-space distribution, with $p(E)$ and $q(E)$ the phase-space weighting factors,

$$p(E) = 4\int_0^{r_{max}(E)} v(r)r^2 dr, \qquad (29a)$$

$$q(E) = \frac{4}{3}\int_0^{r_{max}(E)} v^3(r)r^2 dr, \qquad (29b)$$

and $v = [2\Phi(r) - 2E]^{1/2}$. Near the binary, where the potential is close to Keplerian, $p(E) \approx 2^{-3/2}\pi G^3 M_{12}^3 |E|^{-5/2}$ and $q(E) = (2^{1/2}\pi/6)G^3 M_{12}^3 |E|^{-3/2}$. $\ln\Lambda \approx \ln(M_{12}/m_\star)$ is the Coulomb logarithm. Henceforth f and N are explicitly defined as mass (not number) densities, and $\mathcal{F}$ is the mass flux into the binary's loss cone.

An equation like (27), in which the J-dependence of f is contained implicitly in $\mathcal{F}(E,t)$, was first written by Bahcall & Wolf (1977). It has since been adopted by a number of other authors to describe the evolution of the distribution of stars, compact objects or dark matter around a single supermassive black hole (Murphy et al. 1991; Merritt 2004; Hopman & Alexander 2006). It is being used for the first time in the present paper to describe the evolution of the stellar distribution about a binary black hole. Since $\mathcal{F}$ scales only as $\sim \log r_{lc}^{-1}$ (equation 26), the ratio of the two terms on the right hand side of equation (27) is not greatly affected by the much greater (in linear extent) size of the loss cone of a binary compared with a single black hole.

The relation between the flux into the binary's loss cone and the rate of change of its semi-major axis a is

$$\frac{d}{dt}\left(\frac{GM\mu}{2a}\right) = -\int \mathcal{F}(E,t)\Delta E dE \qquad (30)$$

with $\mu \equiv M_1 M_2/M$, the binary reduced mass and $\Delta E(E)$ the mean specific energy change of stars, originally at energy E, that interact with the binary. In Paper II, we set

$$\Delta E = \Delta E_{\text{Hills}} = -\langle C \rangle \frac{G\mu}{a}, \qquad (31a)$$

$$s(t) \equiv \frac{d}{dt}\left(\frac{1}{a}\right) = \frac{2\langle C \rangle}{aM}\int \mathcal{F}(E,t)dE. \qquad (31b)$$

The coefficient $\langle C \rangle$ is independent of energy for stars that interact with a "hard" binary (Hills 1983; Mikkola & Valtonen 1992; Quinlan 1996a). Hardness is defined as V_{bin}/σ, where $V_{bin} = \sqrt{GM_{12}/a}$ is the relative velocity of the components of the binary and σ is the stellar velocity dispersion in the unperturbed galaxy. An equal-mass binary is in the "hard" regime when $V_{bin}/\sigma \gtrsim 3$ (Quinlan 1996a). In the current models,

$$\frac{V_{bin}}{\sigma_p} \approx 0.36\left(\frac{1}{a}\right)^{1/2} \qquad (32)$$

with $\sigma_p \approx 0.278$ the peak velocity dispersion in the $\gamma = 0.5$ Dehnen model. The N-dependent phase of binary evolution begins at $a^{-1} \approx 100$ in the N-body models (Fig. 6), hence $V_{bin}/\sigma_p \gtrsim 3.6$ and equation (31) is expected to be accurate. In Paper II, setting $\langle C \rangle \approx 1.25$ was found to reproduce the N-body hardening rates. Yu (2002) argued for a similar value of $\langle C \rangle$.

Expressions like (31a) were derived from scattering experiments that allowed for the possibility of multiple interactions between star and binary. However the confining effect of the galaxy's gravitational potential was ignored. As noted in Milosavljević & Merritt (2003), stars ejected once by the binary can interact with it again as they return to the nucleus on nearly-radial orbits. If the energy change during the first interaction is not large enough to eject the star completely from the galaxy, it will experience one or more "secondary slingshots", and the total energy extracted from the binary by the star will be the sum of the discrete energy changes during the interactions.
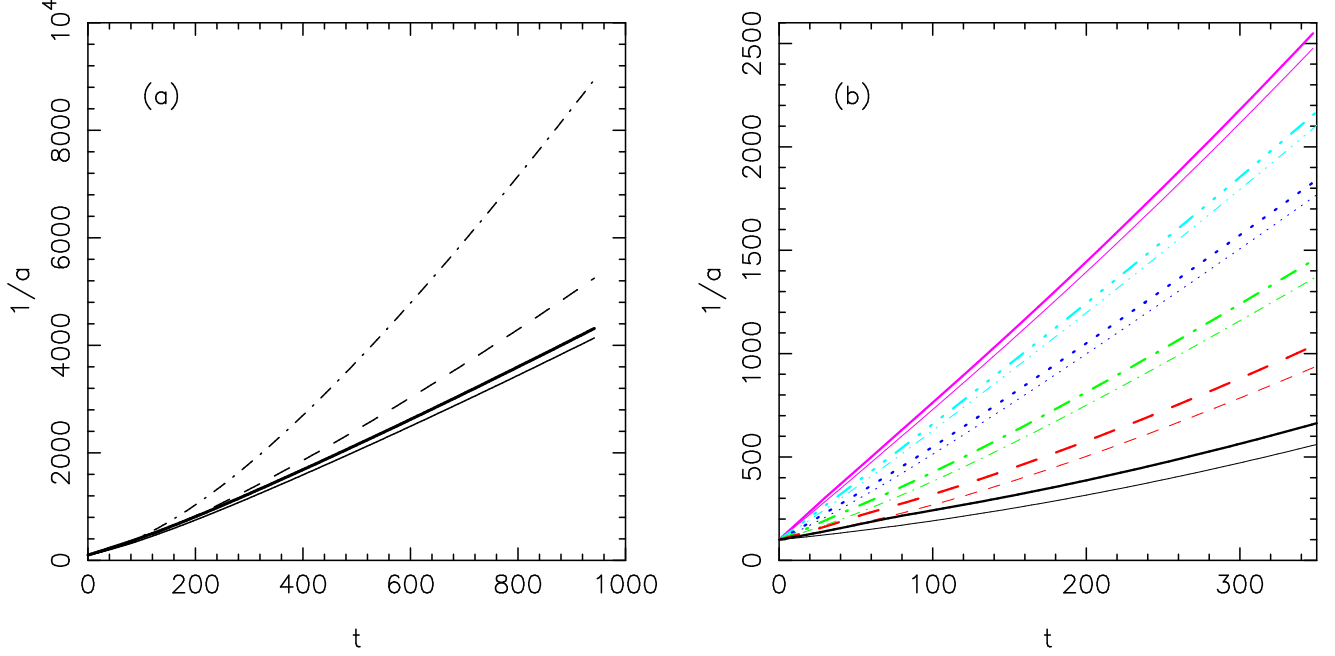
FIG. 14.— (a) Fokker-Planck evolution of binary semi-major axis in a set of integrations designed to mimic the *N*-body simulations with *N* = 65k. *Dot-dashed line:* fixed potential and density; *dashed line:* fixed potential, evolving density; *thin solid line:* evolving density and potential, no re-ejections; *thick solid line:* evolving density and potential with re-ejections. (b) Fokker-Planck integrations with parameters chosen to mimic the *N*-body simulations with various *N*; color coding is the same as in the *N*-body figures above. *Thin lines:* no re-ejections; *solid lines:* with re-ejections.
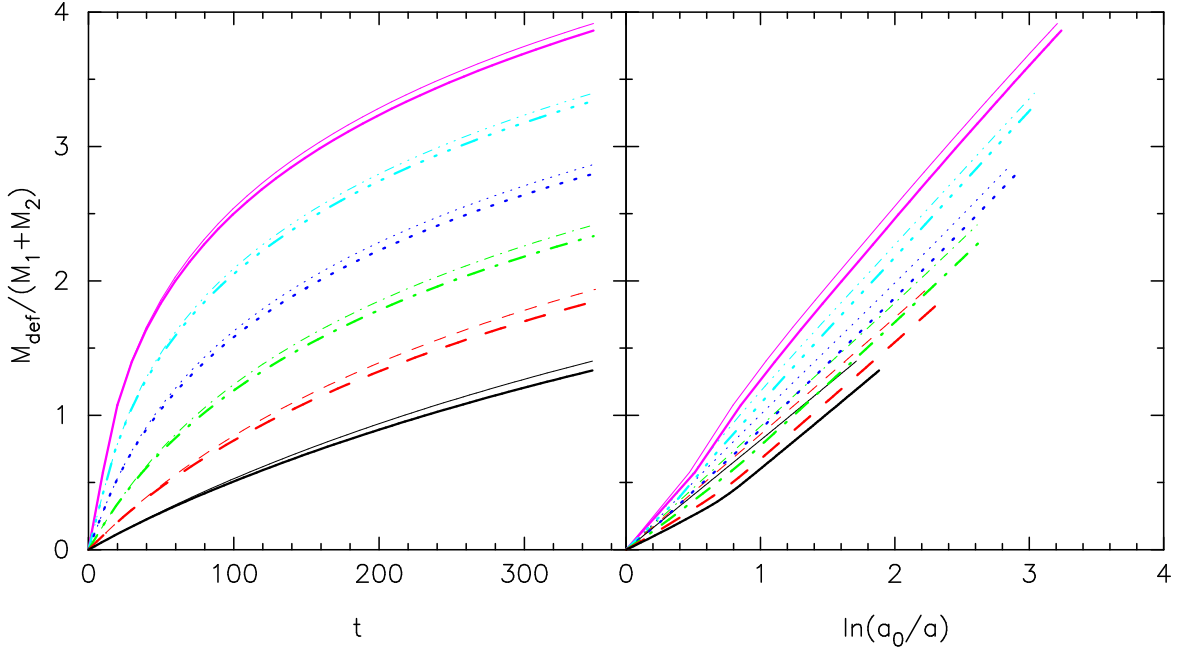

FIG. 15.— Evolution of the mass deficit in the suite of Fokker-Planck integrations presented in Fig. 14. Line styles have the same meaning as in Figure 6.

A minimum condition for re-ejection is that a star remain bound to the galaxy after its first interaction with the binary, $E + \Delta E \gtrsim 0$. Most stars that interact with the binary have apocenters $\sim r_h$ (Milosavljević & Merritt 2003); since the gravitational potential at this radius is dominated by the galaxy, we can write this condition for re-ejection as $|\Delta E| \lesssim \Phi_\star(0)$ with $\Phi_\star(0)$ the central value of the galaxy's (stellar) gravitational potential. The $\gamma = 0.5$ Dehnen models used here have $\Phi_\star(0) \approx 0.67$ in the adopted units, implying $a^{-1} \lesssim 200$ for re-ejection.

Even if a star satisfies this condition, re-ejection will only be effective if the star remains in the binary's loss cone for longer than an orbital period, i.e. if $q(E) \lesssim 1$. Re-ejection will also fail for a star with apocenter greater than some $r_{max} \gg r_h$, since the overall potential in a real galaxy is never precisely spherical and the star will be perturbed from its nearly radial orbit on the way in or out Vicari et al. (2006).

We considered a modified form of equation (31) that accounts for re-ejections. Let $\Delta E_{max} = \Phi(r_{max}) - \Phi(r_h)$. Re-ejection was assumed to occur if the following conditions were both satisfied: (i) $|\Delta E_{\mathrm{Hills}}| < |\Delta E_{max}|$; (ii) $q(E + \Delta E_{\mathrm{Hills}}) < q_{max} \approx 1$. Condition (i) guarantees that the star

remains bound to the galaxy after the first ejection, with apocenter $\leq r_{max}$. This condition is roughly equivalent to $G\mu/a < \Phi_{gal}(0) \approx 1$ and is satisfied for $a^{-1} \lesssim 500 \approx 5a_h^{-1}$ in our models, i.e. during the early phases of binary evolution. Condition (ii) guarantees that the star will remain within the binary loss cone for of order one orbital period or longer after the first ejection; this condition is satisfied at large (i.e. bound) values of E (Fig. 13).

For a^{-1} greater than ~ 160, which occurs shortly after formation of a hard binary (Fig. 5), even a single re-ejection would give a star enough energy to escape the galaxy. Hence, at energies such that conditions (i) and (ii) were both satisfied, we set $\Delta E = 2\Delta E_{\mathrm{Hills}}$, while if either condition was not satisfied, re-ejection was assumed not to occur and we set $\Delta E = \Delta E_{\mathrm{Hills}}$. This scheme has two parameters, q_{max} and r_{max}; the results are weakly dependent on r_{max} for $r_{max} \gg r_h$ and we fixed $r_{max} = 100r_h$. The consequences of varying q_{max} are discussed below.

Finally, we need to account for changes in the gravitational potential as the stellar distribution evolves. (We ignore possible changes in the mass of the binary.) Here we follow Hénon's (1961) scheme of assuming that f remains a fixed function of the radial adiabatic invariant as the potential is adjusted. Our numerical schemes for advancing f was based closely on the algorithms described by Cohn (1980) and Quinlan (1996b).

5.3. *Comparison with the N-Body Integrations*

Figure 14(a) compares the evolution of a^{-1} in a set of Fokker-Planck integrations with initial conditions chosen to mimic those in the N-body integrations ($\gamma = 0.5$, $M = 0.01$, $a^{-1}(t=0) = 0.01$). Fixing $\rho(r)$ and $\Phi(r)$ (dot-dashed curve) is equivalent to the assumptions made by Yu (2002), who ignored changes in the stellar distribution as the binary evolved. Allowing the density and potential to evolve (solid lines) results in a considerably lower hardening rate for the binary. Including the secondary-slingshot (heavy solid line) increases the hardening rate but only slightly; as explained above, once the binary becomes hard, most stars that interact with it are ejected completely from the galaxy and do not return to the binary's sphere of influence.

Figure 14(b), which can be compared with Figure 6(b), shows the evolution of binary semi-major axis in a set of Fokker-Planck integrations with the same values of N as in the N-body integrations. The correspondence is quite good; the Fokker-Planck integrations show a slightly steeper dependence of the binary hardening rate on N (Fig. 8). The evolution of the mass deficit as derived from the Fokker-Planck integrations is shown in Figure 15 (cf. Fig. 11). Here the correspondence is not quite as good, but still reasonable; the weak dependence of M_{def} on N for large N is well reproduced.

6. PREDICTIONS OF THE FOKKER-PLANCK MODEL FOR LARGE N

Having established that the Fokker-Planck model can mimic the joint binary/galaxy evolution seen in the N-body integrations, for various values of $N \lesssim 10^5$, we now extend this model to the much larger N regime of real galaxies. The goal is both to predict the long-term evolution of a massive binary in a real galaxy, and also to record the changes in the central structure of the galaxy.

Results for a galaxy containing a binary with $M_{12} \equiv M_1 + M_2 = 10^{-3}M_{\mathrm{gal}}$ and two mass ratios $\alpha \equiv M_2/M_1 = (1,0.1)$ are shown in Figures 16 and 17 respectively. The initial

galaxy model was a Dehnen sphere, equation (10), with $\gamma = 0.5$. This is the shallowest central slope that is consistent with an isotropic phase-space distribution around a central point mass; it is also a fair representation of the core profiles that are produced during the "rapid" phase of cusp destruction that accompanies the initial formation of the massive binary (Merritt & Szell 2006). Fokker-Planck integrations were carried out for different values of $N \equiv M_{\mathrm{gal}}/m_\star = (10^6, 10^7, ..., 10^{12})$. The time axis in these plots is the relaxation time measured at the binary's influence radius in the initial model; all integrations were continued until $t = 4T_r(r_h)$. Equation (12) was used to set the initial value of a; quantities like the mass deficit in Figures 16 and 17 should be interpreted as the accumulated change in these quantities after the binary first becomes "hard." Unless otherwise stated, re-ejections were ignored.

In all of the integrations, the binary begins in the diffusive, or empty loss cone, regime ($q_{lc} \gg 1$) due to its large initial separation, and evolves toward the pinhole, or full loss cone, regime ($q_{lc} \gtrsim 1$) as it hardens. The transition to the pinhole regime occurs later for larger N; for $N = 10^{12}$ (the heavy curves in Figs. 16 and 17) the binary remains essentially in the diffusive regime until the end of the integration at $4T_r(r_h)$. However we argue below that evolution of binaries in real galaxies would typically be expected to terminate before the pinhole regime is reached.

6.1. *Binary Hardening Rates*

Figures 16 and 17 show that at large N, the binary hardening time,

$$T_{\mathrm{hard}} \equiv \left| \frac{a}{\dot{a}} \right|, \qquad (33)$$

tends to a fixed fraction of $T_r(r_h)$ at any given a. This is the "empty loss cone" regime. The ratio $T_{\mathrm{hard}}/T_r(r_h)$ increases from ~ 0.1 at large a, i.e. early times, to ~ 0.3 when $a \approx 10^{-5}a_h$, with a weak dependence on binary mass ratio. We will argue below that binary black holes in real galaxies lie close to the large-N hardening curves throughout much of their evolution and so it is of interest to develop an analytic understanding of this regime.

Since $q_{lc}(E)$ (equation 22) is the ratio of the orbital period to the diffusional loss cone refilling time at energy E, i.e. $q_{lc}(E) \approx P(E)/[R_{lc}(E)T_r(E)]$, we can rewrite the flux of stars into the binary, equation (26), as

$$\mathcal{F}(E)dE \approx 4\pi^2 J_c^2(E)P(E)T_r^{-1}(E)\frac{\overline{f}(E)}{\ln(1/R_0)-1}dE. \quad (34)$$

Assuming a fixed mass model for the galaxy, the flux into the binary, integrated over one relaxation time, scales therefore as

$$\mathcal{F}(E)T_r(E) \propto [\ln(1/R_0)-1]^{-1} \qquad (35a)$$

$$\approx \left[\ln R_{lc}^{-1}\right]^{-1}, \quad q_{lc} \ll 1; \qquad (35b)$$

$$\approx q_{lc}^{-1}, \qquad q_{lc} \gg 1. \qquad (35c)$$

The binary hardening rate is fixed by $\mathcal{F}$ and a (equation 31b), so these expressions imply that the binary's evolution over a specified number of relaxation times will be smaller for smaller N, i.e. larger q_{lc}; while in the large-N limit, the evolution rate at a given a will be determined solely by T_r. These predictions are consistent with the upper panels of Figures 16 and 17.
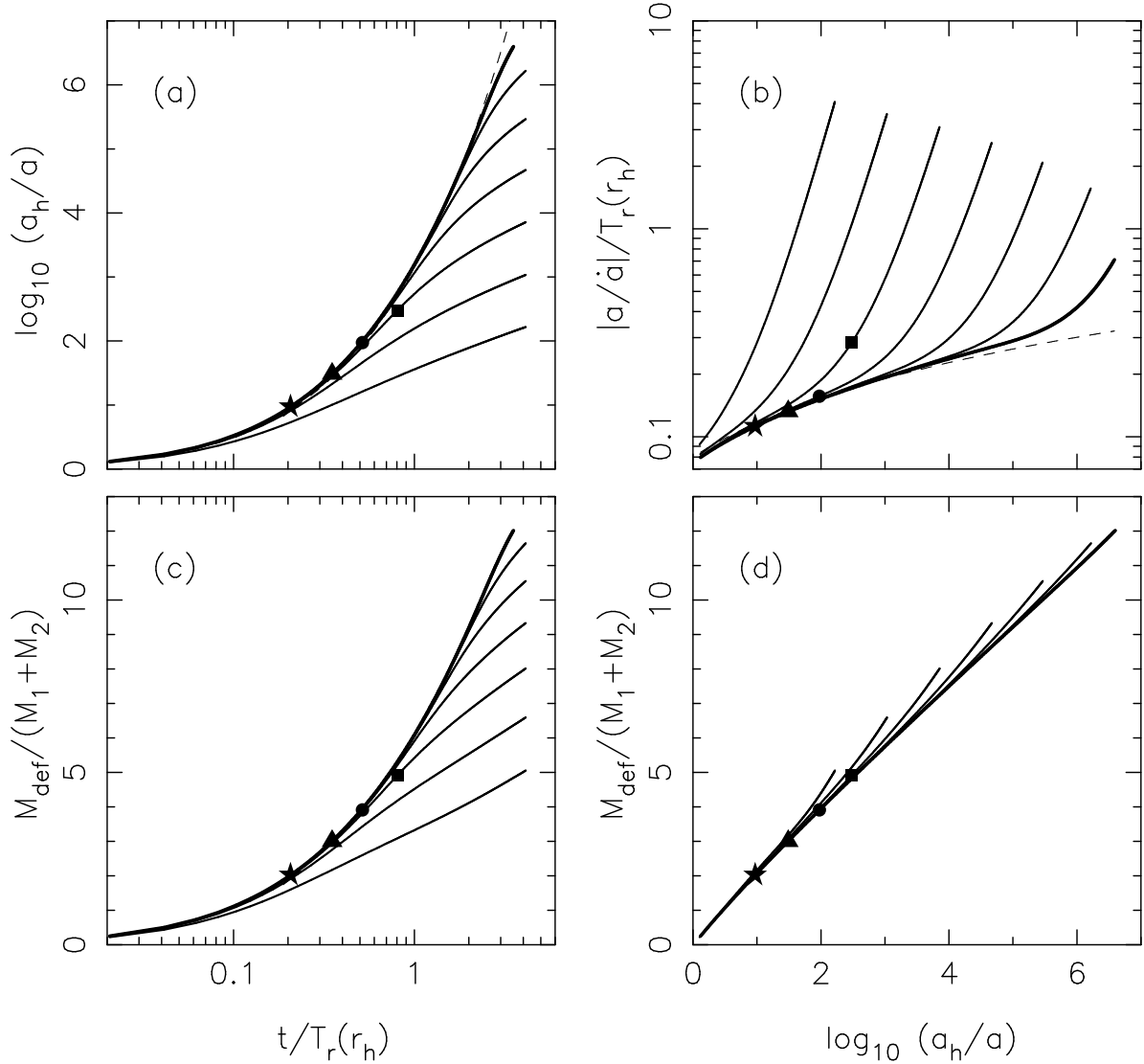
FIG. 16.— Joint binary-galaxy evolution in Fokker-Planck models with $M_1 = M_2$ and $M_{12} = 10^{-3}M_{gal}$. (a) Binary semi-major axis; (b) binary hardening time; (c) mass deficit as a function of time, and (d) mass deficit as a function of binary separation. Different lines correspond to different values of $N \equiv M_{gal}/m_\star$: $N = 10^6, 10^7, ..., 10^{11}, 10^{12}$ (thick line). Symbols mark the time t_{eq} at which the binary hardening rate equals the gravitational radiation evolution rate, assuming a binary mass of $10^5 M_\odot$ (squares), $10^6 M_\odot$ (circles), $10^7 M_\odot$ (triangles), and $10^8 M_\odot$ (stars). Filled symbols denote models in which N is roughly equal to its value in real galaxies, for each value of $M_\bullet$. Dashed lines in panels (a) and (b) are the analytic model described in the text.

The gradual decrease with time of the hardening rate is due to two factors: the decreasing size of the binary, and the declining density of the core. Again ignoring changes in the core structure, the expressions given above can be used to estimate how the hardening rate varies with a. The result, in the large-N limit, is

$$\frac{1}{T_r}\left|\frac{a}{\dot{a}}\right| \equiv \frac{T_{hard}}{T_r} \propto \ln\left(\frac{a_h}{a}\right), \qquad (36)$$

i.e. the fractional change in a over one relaxation time is weakly dependent on a for large N.

We tried fitting a similar function to the large-N hardening curves in Figures 16 and 17, i.e.

$$\frac{1}{T_r}\left|\frac{a}{\dot{a}}\right| = A\ln\left(\frac{a_h}{a}\right) + B. \qquad (37)$$

The results are shown as the dashed lines in Figures 16b and 17b. We found good fits for

$$A = (0.016, 0.017), \qquad B = (0.08, 0.09) \qquad (38)$$

for $\alpha = (1, 0.1)$ respectively. The weak dependence of the fitting parameters on binary mass ratio reflects the lack of a mass ratio dependence in the evolution equations (31).

Integrating equation (37) gives a simple expression for the time dependence of the binary semi-major axis:

$$\ln\left(\frac{a_h}{a}\right) = -\frac{B}{A} + \sqrt{\frac{B^2}{A^2} + \frac{2}{A}\frac{t}{T_r(r_h)}} \qquad (39)$$

where t is defined, as in Figures 16 and 17, as the time since the binary first became hard, i.e. the time since $a = a_h$. This function is plotted in Figures 16a and 17a, where it again provides an excellent fit to the large-N evolution curves.

We now show that real black hole binaries are expected to be in this empty loss cone regime throughout most or all of their evolution. Maximum traversal of the tracks in Figures 16 and 17 will occur if no physical process, aside from interactions with stars, affects the hardening rate until the gravitational radiation regime is reached. The time scale associated
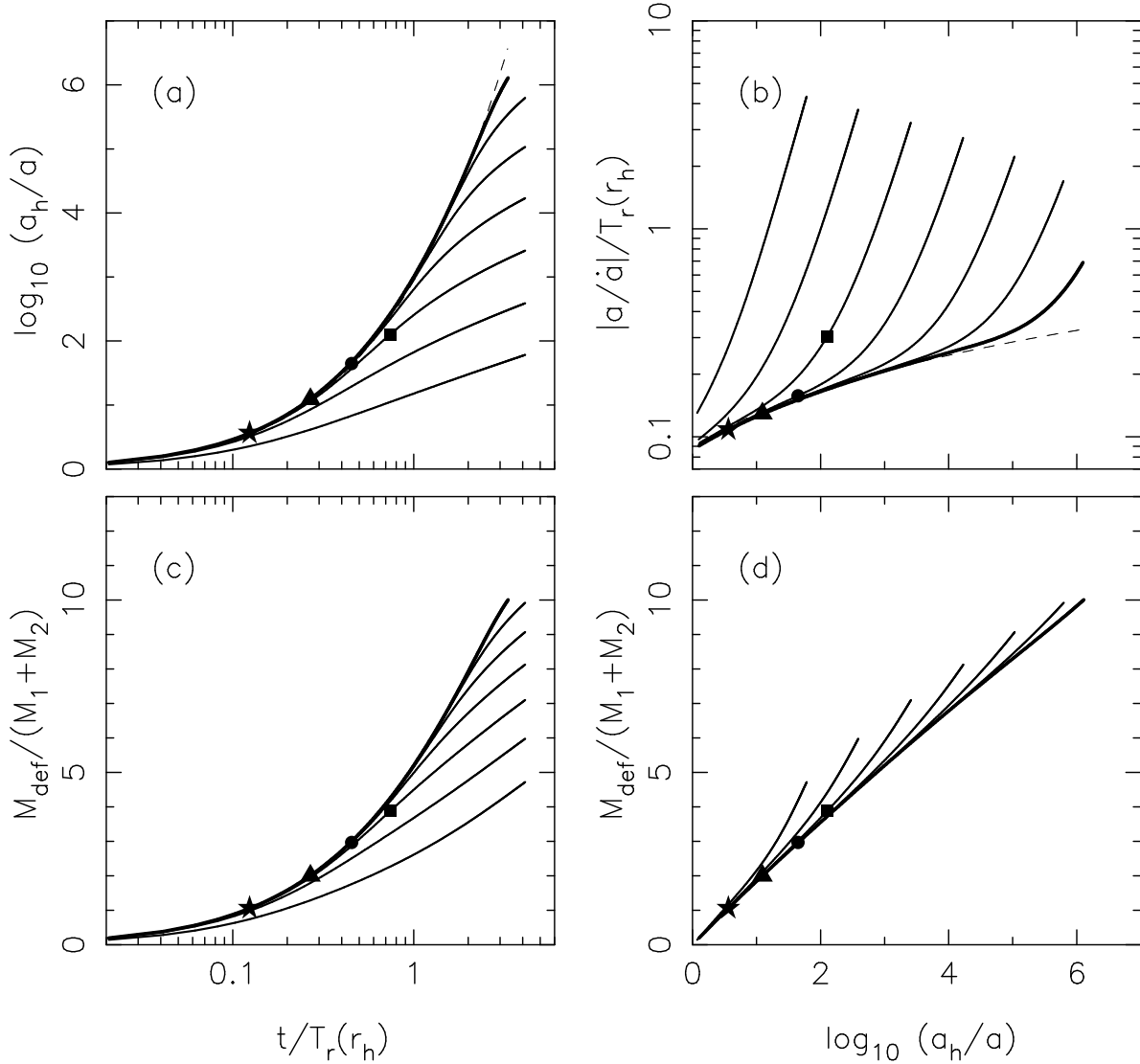
FIG. 17.— Like Fig. 16 but for $M_2 = 0.1M_1$ and $M_{12} = 10^{-3}M_{\rm gal}$.

with gravitational radiation is (Peters 1964)

$$T_{\rm gr} = \left| \frac{a}{\dot{a}} \right|_{\rm gr} = \frac{5}{64} \frac{c^5}{G^3} \frac{a^4}{\mu M_{12}^2} \qquad (40)$$

where $\mu \equiv M_1 M_2 / M_{12}$ is the reduced mass of the binary and a circular orbit has been assumed. Following Merritt & Milosavljević (2005), $T_{\rm gr}$ can be expressed in terms of $M_\bullet \equiv M_{12}$ and a_h using the $M_\bullet - \sigma$ relation, equation (3), as

$$T_{\rm gr} \approx 5.7 \times 10^{10} {\rm yr} \frac{\alpha^3}{(1+\alpha)^6} M_{\bullet,6}^{-0.65} \tilde{a}_{-2}^4 \qquad (41)$$

with $\tilde{a} \equiv a/a_h$ and $\tilde{a}_{-2} = a/(0.01 a_h)$.

We define t_{eq} as the time when $T_{\rm hard} = T_{\rm gr}$. In order to extract t_{eq} in physical units from the Fokker-Planck integrations, we need to assign a value in years to $T_{\rm r}(r_h)$. This we do via the straight-line fit to the data in Figure 1. Combining equations (4), (37), and (41) the condition $T_{\rm hard} = T_{\rm gr}$ becomes

$$\left(\frac{a_h}{a} \right)^4 \left[A \ln \left(\frac{a_h}{a} \right) + B \right] = 7.1 \times 10^8 \alpha^3 (1+\alpha)^{-6} M_{\bullet,6}^{-2.19}$$
$$(42)$$

with $M_{\bullet,6} \equiv M_\bullet / 10^6 M_\odot$. We define $a_{\rm eq}$ as the value of a that satisfies this equation. For $M_\bullet = (10^5, 10^6, 10^7, 10^8) M_\odot$, i.e.

$\sigma \approx (44, 70, 112, 180)$ km s^{-1}, and using the values of A and B derived above, equation (42) implies

$$a_h / a_{\rm eq} \approx (315, 93, 27, 8.0) \qquad (43)$$

for $\alpha \equiv M_2 / M_1 = 1$, and

$$a_h / a_{\rm eq} \approx (140, 40, 12, 3.5) \qquad (44)$$

for $\alpha = 0.1$. The corresponding times are

$$t_{eq} \approx (0.73, 0.53, 0.35, 0.20) \times T_{\rm r}(r_h)(\alpha = 1), \qquad (45)$$
$$\approx (0.65, 0.54, 0.27, 0.13) \times T_{\rm r}(r_h)(\alpha = 0.1). \qquad (46)$$

The values just computed for a_{eq} and t_{eq} correspond to the large-N (empty loss cone) limit of the Fokker-Planck equation, i.e. to the heavy curves in Figures 16 and 17. The filled symbols in those figures show where $T_{\rm hard} = T_{\rm gr}$ on the four tracks that best correspond to the four values just considered for $M_\bullet$. Since $M_\bullet \approx 1 \times 10^{-3} M_{gal}$ (Merritt & Ferrarese 2001), we set $N = (10^8, 10^9, 10^{10}, 10^{11})$ for $M_\bullet = (10^5, 10^6, 10^7, 10^8) M_\odot$. The symbols confirm that binary black holes of mass $M_\bullet \gtrsim 10^{5.5} M_\odot$ remain essentially in the empty loss cone regime throughout their evolution. For binaries of mass $M_\bullet = 10^5 M_\odot$, the evolution just prior to the

gravitational radiation regime begins to depart from that of a diffusive loss cone, resulting in somewhat lower hardening rates than predicted by equations (37) and (39). The discrepancy with the analytic expressions would be expected to increase still more for binaries of still lower mass (if such exist).

6.2. *Mass Deficits*

Next we consider the effect of the binary on the structure of the galaxy's core. Evolution of mass deficits is plotted in the lower panels of Figures 16 and 17. Particularly striking are the panels showing M_{def} vs. binary hardness, a_h/a. As was true in the N-body integrations, long-term evolution of the binary generates mass deficits that are very well predicted by the change in binding energy of the binary black hole, i.e. by a_h/a. This dependence is accurately described by

$$\frac{M_{\text{def}}}{M_{12}} \approx (1.8, 1.6) \log_{10}(a_h/a) \qquad (47)$$

where the numbers in parentheses refer to $\alpha = (1, 0.1)$ respectively. The mass deficits generated between formation of a hard binary, and the start of the gravitational radiation regime, are given by setting $a = a_{\text{eq}}$ in this expression, i.e.

$$M_{\text{def}} \approx (4.5, 3.5, 2.6, 1.6) M_{12} \quad (\alpha = 1) \qquad (48)$$
$$\approx (3.4, 2.6, 1.7, 0.9) M_{12} \quad (\alpha = 0.1). \qquad (49)$$

for $M_{12} = (10^5, 10^6, 10^7, 10^8) M_\odot$. These values should be added to the mass deficits $M_{\text{def,h}}$ generated during the rapid phase of binary formation, i.e. $M_{\text{def,h}} \approx 0.7\alpha^{0.2} M_{12}$ (Merritt 2006).

Mass deficits in these models are not related in a simple way to the mass in stars "ejected" by the binary. The flux of stars into the binary constitutes a loss term, $-\mathcal{F}(E,t)$, on the right hand side of equation (27), and in the absence of any other influences, the density of stars near the center of the galaxy would drop in response to this term. Removal of stars also reduces the gravitational force near the center, contributing to the expansion. However the second term on the right hand side of equation (27), $-\partial F_E/\partial E$, has the opposite effect. This term represents the change in $N(E,t)$ due to diffusion of stars in energy; as the mass deficit increases, so do the gradients in f, which tend to increase the energy flux and counteract the drop in density.

In principle, these two terms could balance, at least over some range in energies, allowing the binary to harden without generating a mass deficit. This would require

$$F_E(E) = \int_E^\infty \mathcal{F}(E) dE, \qquad (50)$$

i.e. the inward flux of stars due to energy diffusion at energy E must equal the *integrated* loss to the binary at all energies greater than E. However, at sufficiently great distances from the binary, the relaxation time is so long that the local $F_E(E)$ must drop below the integrated loss term, implying that the density within this radius will drop. Growth of a mass deficit reflects the imbalance between these two terms.

We illustrate this imbalance in Figure 18 which shows $F_E(E)$ and $\int \mathcal{F}(E) dE$ in the Fokker-Planck integration with $\alpha = 1$ at a time $\sim T_r(r_h)$. The lowest energy in the figure corresponds roughly to the outer edge of the binary-generated core.

Yet another mechanism contributes to the growth of mass deficits in the Fokker-Planck models. Even in the absence of the loss term associated with the binary, the nuclear density
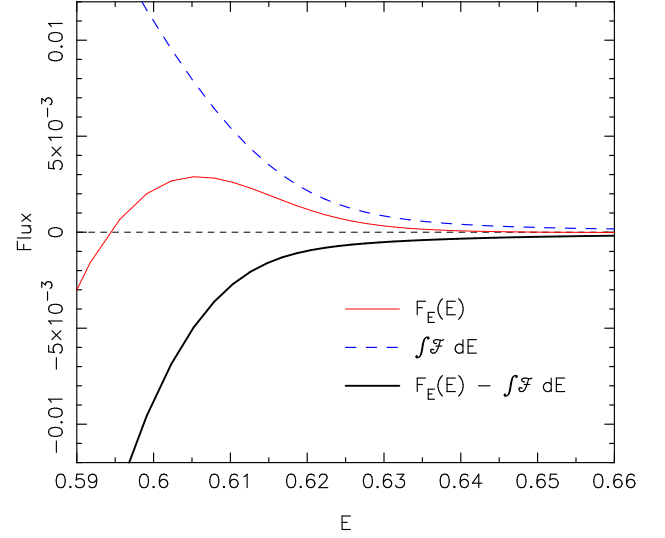

FIG. 18.— Fluxes in the Fokker-Planck integration with $N = 10^7$ and $\alpha = 1$, at a time $\sim T_r(r_h)$.

profile adopted here for the initial models, $\rho \sim r^{-0.5}$, implies a "temperature inversion," i.e. a velocity dispersion that increases with radius. Relaxation drives such a nucleus toward a locally "isothermal" form before the onset of core collapse, causing the central density to drop (Quinlan 1996b). The binary contributes to this process by maintaining a flat density profile near the center, forcing the temperature inversion to persist.

7. IMPLICATIONS FOR BINARY EVOLUTION IN GALAXIES

Equation (39), based on the Fokker-Planck integrations, accurately describes the evolution of a hard binary in the empty loss cone regime (i.e. in galaxies with $M_{12} \gtrsim 10^{5.5} M_\odot$) given the relaxation time at r_h, while equation (4), based on observed properties of galactic nuclei (Fig. 1), provides the mean value of $T_r(r_h)$ for galaxies with black hole mass $M_\bullet = M_{12}$. Together with equation (40) for the gravitational radiation time scale, these relations can be used to predict mean evolution rates and binary separations in real galaxies given $(M_\bullet, \alpha) \equiv (M_2/M_1)$.

Including the effect of energy lost to gravitational radiation, the binary's semi-major axis evolves as

$$\frac{d}{dt}\left(\frac{1}{a}\right) = \frac{d}{dt}\left(\frac{1}{a}\right)_{\text{hard}} + \frac{d}{dt}\left(\frac{1}{a}\right)_{\text{gr}} \qquad (51)$$

i.e.

$$T(a)^{-1} \equiv a\frac{d}{dt}\left(\frac{1}{a}\right) = T_{\text{hard}}^{-1}(a) + T_{\text{gr}}^{-1}(a). \qquad (52)$$

The time for the separation to drop from a_h to a is

$$10^{10}\text{yr} \times \int_0^{y_{max}} \frac{Ay + B}{C + D(Ay + B)e^{4y}} \qquad (53)$$

where

$$C = 1.25 M_6^{-1.54}, \qquad (54a)$$
$$D = 1.75 \times 10^{-9}\alpha^{-3}(1 + \alpha)^6 M_6^{0.65} \qquad (54b)$$

and $y_{max} = \ln(a_h/a)$. The full time to coalescence, t_{coal}, starting from a_h is given by setting $y_{max} = \infty$ in this expression. Figure 19 shows t_{coal} as a function of M_{12} for $\alpha = (1, 0.1)$. Shown separately on this figure is the time to evolve from
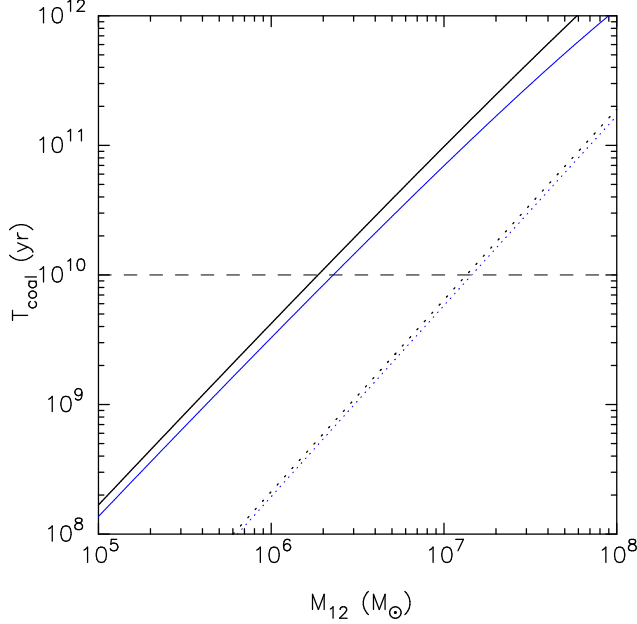
FIG. 19.— Time to coalescence starting from $a = a_h$ as a function of binary mass. Solid curves are derived from equation (53) with $y_{max} = \infty$; black/thick: $\alpha = 1$; blue/thin: $\alpha = 0.1$. Dotted curves show the evolution time from $a = a_{eq}$ to $a = 0$, i.e. the time spent in the gravitational radiation regime only. Equation 55 gives accurate analytic approximations to $t_{coal}(M_{12};\alpha)$.

$a = a_{eq}$ to $a = 0$, i.e. the time spent in the gravitational radiation regime alone. The latter time is a factor ~ 10 shorter than the total evolution time t_{coal}, which motivates fitting the following functional form to $t_{coal}(M_{12};\alpha)$:

$$Y = C_1 + C_2 X + C_3 X^2, \tag{55a}$$

$$Y \equiv \log_{10}\left(\frac{t_{coal}}{10^{10}\text{yr}}\right), \tag{55b}$$

$$X \equiv \log_{10}\left(\frac{M_{12}}{10^6 M_\odot}\right). \tag{55c}$$

(This functional form is the integral of equation 39.) A least-squares fit to the curves in Figure 19 gives

$$\alpha = 1: C_1 = -0.372, C_2 = 1.384, C_3 = -0.025 \tag{56a}$$
$$\alpha = 0.1: C_1 = -0.478, C_2 = 1.357, C_3 = -0.041 \tag{56b}$$

The fit of the analytic expressions is better than 2% ($\alpha = 1$) and 5% ($\alpha = 0.1$); most of the deviations occur at the high-M_{12} end where coalescence times are much longer than a Hubble time.

Based on Figure 19, binary black holes would be expected to reach gravitational wave coalescence in 10 Gyr in galaxies with $M_{12} \lesssim 2 \times 10^6 M_\odot$.

Figure 20 shows the probability predicted by equation (52) of finding the binary in a unit interval of $\ln a$,

$$P(\ln a) \propto a \left|\frac{da}{dt}\right|^{-1} \propto T(a), \tag{57}$$

for four values of M_{12} and for $\alpha = (1, 0.1)$. Viewed at a random time before coalescence, a hard binary is most likely to be seen at $a \approx 2a_{eq}$, although the distributions are nearly flat for $1 \leq a_h/a \lesssim 2a_h/a_{eq}$. For $M_{12} \gtrsim 10^7 M_\odot$, evolution for 10 Gyr would only bring the binary separation slightly below a_h; in these galaxies the most likely separation to find a binary would be the stalling radius (Merritt 2006).
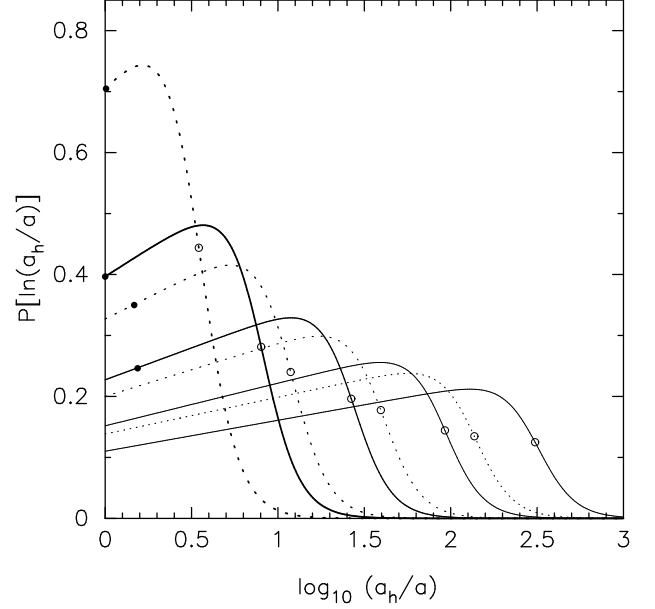

FIG. 20.— Probability of finding a binary black hole in a unit interval of $\ln a$. From left to right, curves are for $M_{12} = (0.1, 1, 10, 100) \times 10^6 M_\odot$. Solid(dashed) curves are for $M_2/M_1 \equiv \alpha = 1(0.1)$. Open circles indicate $a = a_{eq}$; filled circles correspond to an elapsed time since $a = a_h$ of 10^{10} yr. For the two smallest values of $M_\bullet$, the latter time occurs off the graph to the right.

8. IMPLICATIONS FOR THE STRUCTURE OF GALAXY CORES

In the most luminous spheroids, mass deficits generated by a binary black hole are likely to persist for the lifetime of the galaxy, since relaxation times are much too long for star-star scattering to alter the phase-space density (cf. Fig. 1). In collisional nuclei on the other hand, relaxation times are short enough that the stellar distribution can be substantially affected by gravitational encounters *after* the binary black hole has coalesced into a single black hole. A Bahcall-Wolf (1976) cusp will form in a time $\sim T_r(r_h)$ after the binary black hole coalesces into a single hole, inside a radius $\sim 0.2r_h$ (Merritt & Szell 2006). In addition, the structure of the nucleus beyond the cusp will continue to evolve, as two-body encounters drive the stellar "temperature" profile toward isothermality prior to the onset of core collapse (Quinlan 1996b). The nuclear density profile at some time after coalescence will depend on how far along the evolutionary tracks of Figs. 16 and 17 the binary evolved before coalescing, as well as on the elapsed time since coalescence.

Figure 21 illustrates these competing effects with a concrete example. A Fokker-Planck integration with $N = 10^9$ and $\alpha = 1$ was carried out until a time $t = t_{eq}$; t_{eq} was computed as above assuming a binary mass of $10^6 M_\odot$. The binary was assumed to become a single black hole at this time; the integration was then continued for a time $T_r(r_h)$, but with the binary loss term $\mathcal{F}(\mathcal{E})$ set to zero. As the figure shows, a $\rho \sim r^{-7/4}$ cusp is generated at $r \lesssim 0.2r_h$. The net result is a flat core containing at its center a compact star cluster around the black hole. The stellar mass within the cusp is $\sim 0.1M_\bullet$.

If binary coalescence were assumed to take place sooner than $\sim t_{eq}$ (due e.g. to gas-dynamical torques), the mass deficit would be smaller than the value $\sim 3.5M_{12}$ generated in this integration, resulting in a nuclear density profile more like those of Merritt & Szell (2006). As shown in that paper, a regenerated cusp can closely approximate the (coreless) density profile at the center of the Milky Way if the elapsed
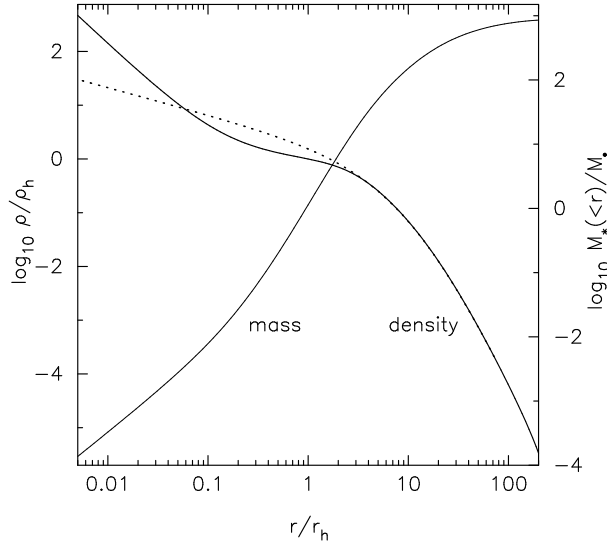
FIG. 21.— Stellar density and mass profiles in a Fokker-Planck integration with $N = 10^9$. The binary black hole was assumed to coalesce at $t = t_{eq}$ (based on an assumed binary mass of $10^6 M_\odot$) and the integration was then continued, without the binary sink term, for one relaxation time at r_h. A Bahcall-Wolf cusp is generated at $r \lesssim 0.2 r_h$; the stellar mass within the cusp is $\sim 0.1 M_\bullet$. Dashed line is the initial galaxy model.

time since binary coalescence is $\gtrsim 8$ Gyr. In the integration of Figure 21, on the other hand, the larger mass deficit is not completely "erased" by formation of the cusp.

A nuclear cusp like that in Figure 21 would be unresolved in all but the nearest galaxies. In fact, recent observations suggest the presence of compact stellar nuclei ("nuclear star clusters") at the centers of most spheroids fainter than $\sim 10^9 L_\odot$ (Rossa et al. 2006; Wehner & Harris 2006; Ferrarese et al. 2006). The mean mass associated with the nuclei is a fraction $\sim 0.2\%$ that of the host galaxy with a $\pm 1\sigma$ range of $0.06\% - 0.52\%$ (Ferrarese et al. 2006). If we assume that low-luminosity spheroids contain massive black holes and that the ratio of black hole mass to spheroid mass is similar to the mean value $\sim 0.12\%$ characteristic of more luminous galaxies (Merritt & Ferrarese 2001), the observed nuclei would have masses that are fractions $0.5 - 4$ that of the black holes. This is somewhat larger than the value $M_{cusp}/M_\bullet \approx 0.1$ in the example of Figure 21; on the other hand it is possible that black holes in faint spheroids carry a larger fraction of the spheroid mass. The compact nuclei might also form in very different ways, e.g. from gas that accumulates at the center.

9. ALTERNATE MODELS FOR BINARY EVOLUTION

Yu (2002) computed evolutionary tracks for binary black holes at the centers of a sample of early-type galaxies for which detailed luminosity profiles were available. Evolution beyond $a \approx a_h$ was modelled using the second term on the right hand side of equation (27), i.e. the J-directed flux of stars into the binary. The stellar distribution function was assumed fixed in time; binary-induced changes in the structure of the nucleus were ignored, as were changes in stellar energy, although the time scales associated with both sorts of change are comparable to the time scale for loss cone repopulation. As shown here (Figure 14), allowing for changes in the structure of the nucleus in a Fokker-Planck model reduces the binary hardening rate by a factor ~ 2. Yu (2002) concluded that binary black holes in spherical galaxies with $\sigma \lesssim 90$ km s^{-1} could coalesce in a Hubble time. This velocity dispersion corresponds to a binary mass of $\sim 3.5 \times 10^6 M_\odot$ (eq. 3). Yu's con-

clusion is consistent with, but slightly more optimistic than, the one reached in the current study (see Fig. 19); the differences are probably due to Yu's neglect of the back-reaction of the binary on the nucleus. As in the current study, Yu found a weak dependence of coalescence time on binary mass ratio.

Some recent studies have inferred rapid evolution of supermassive binary black holes at the centers of spherical galaxies, even in the absence of collisional loss-cone repopulation. Sesana et al. (2007) used detailed three-body scattering experiments to evaluate the effectiveness of the "secondary slingshot" (Milosavljević & Merritt 2003) at extracting energy from massive binaries after they had reached the stalling radius $a \approx a_h$ in spherical galaxies. They found that binaries could shrink beyond a_h by factors of $\sim 4(2)$ for mass ratios of $1(0.1)$; for mass ratios below ~ 0.01 the secondary slingshot was found to be ineffective. Almost all of this evolution took place within a few galaxy crossing times after the hard binary had formed; after this time, all of the stars that were originally within the binary's loss cone had been completely ejected from the galaxy.

In spite of this very modest evolution, Sesana et al. (2007) concluded that "even in the absence of other mechanisms driving orbital decay, pairs involving genuinely supermassive holes [i.e. with combined mass $\gtrsim 10^5 M_\odot$] should not stall". This optimistic conclusion appears to have been based on an evaluation of the mass "ejected" by the binary (their Fig. 5), rather than on the more fundamental criterion of binary separation. The time to coalescence once a binary reaches the gravitational radiation regime is $1/4$ of the time T_{gr} defined in equation (41); coalescence occurs in a time of t_9 Gyr if

$$\frac{a}{a_h} \approx (0.015, 0.034) \times M_{\bullet,6}^{0.16} t_9^{0.25} \qquad (58)$$

where the numbers in parentheses correspond to $\alpha = (1, 0.1)$ respectively. The a/a_h values in equation (58) are ~ 15 times smaller than those found by Sesana et al. (2007) after the secondary slingshot had run its course, implying that the binaries in their model galaxies would stall at separations far outside the gravitational radiation regime unless extremely eccentric.

Sesana et al. (2007)'s results might still be taken to imply that massive binaries commence their long-term, relaxation-driven evolution starting from separations somewhat smaller than $\sim a_h$, as assumed here. However such an effect was not apparent in the fully self-consistent N-body simulations of Merritt (2006). This is probably due to the neglect by Sesana et al. of the changes in nuclear structure that accompany binary formation. Sesana et al. computed the initial population of stars available to undergo reejections by assuming a singular isothermal sphere density profile, $\rho \propto r^{-2}$, and counting the number of stars on orbits that intersected the binary. Even if such a steep density profile were present intially, it would be converted into a core of much lower density by the time $a \approx a_h$, and the number of stars available for the secondary slingshot would be much less than Sesana et al. estimated.

In the Fokker-Planck integrations presented here (§5), the inclusion of the secondary slingshot had almost no effect on the long-term behavior of $a(t)$.

Zier (2006a,b) also argued that stars near a binary black hole at the time of its formation could drive the binary to the gravitational radiation regime in a very short time. Zier ignored the secondary slingshot, but assumed that a dense cluster of stars would be bound to the binary at the time that its separation first reached $\sim a_h$. He found that a cluster having total mass $\sim M_{12}$, distributed as a steep power-law around the

binary, $\rho \sim r^{-\gamma}$, $\gamma \gtrsim 2.5$, could extract enough energy from it via the gravitational slingshot that T_{gr} would fall below 10^{10} yr. While no detailed justification for such dense massive clusters was presented, Zier argued that "Low angular momentum matter accumulates in the center" of merging galaxies, and that "Each of the BHs will carry a stellar cusp with a mass of about its own" after the merger. As noted above, recent observations do suggest the presence of compact nuclei at the centers of low-luminosity spheroids.

N-body simulations of Zier's model have yet to be carried out, although Milosavljević & Merritt (2001) did follow the evolution of merging galaxies with initial, $\rho \sim r^{-2}$ cusps around each of the black holes, close to the value $\gamma = 2.5$ above which Zier infers rapid coalescence. Milosavljević & Merritt (2001) observed a rapid phase of evolution of the binary, during which the density cusps were destroyed and a dropped by a factor of $\sim$ a few below a_h. However this was still far above the separation at which gravitational radiation would be efficient.

An early, heuristic model for binary evolution was presented by Merritt (2000) based on the results of the N-body experiments that had been carried out up to that date. The model assumed that the rate of supply of stars to the binary was determined by local parameters (density, velocity dispersion) and was independent of the nuclear relaxation time. The model was able to mimic the binary hardening rates seen in some N-body experiments (Quinlan & Hernquist 1997; Chatterjee, Hernquist & Loeb 2003); when scaled to real galaxies, it predicted binary coalescence times that were nearly independent of galaxy mass. However, the N-body results on which the model was based were subsequently called into question when they could not be reproduced using more accurate integrators (Makino & Funato 2004; Berczik, Merritt & Spurzem 2005). M. Volonteri and co-authors adopted the Merritt (2000) prescription for binary evolution as a component of their semi-analytic models of black hole growth (Volonteri et al. 2003a,b, 2005), and their models can therefore be expected to substantially over-estimate the rate of binary evolution in galaxies with $M_\bullet \gtrsim 10^7 M_\odot$.

10. SUMMARY

1. Accurate, long-term N-body integrations of binary supermassive black holes at the centers of realistically dense galaxy models were carried out using particle numbers up to

0.26×10^6. A new implementation of the Mikkola-Aarseth chain regularization algorithm was used to treat close interactions involving the black hole particles. The dependence of the binary's hardening rate on particle number was quantified by averaging the results of independent integrations.

2. A Fokker-Planck model was developed that includes, for the first time, changes in the stellar density and potential due to star-binary interactions. The Fokker-Planck model was verified by comparison with the averaged N-body integrations.

3. Based on the Fokker-Planck integrations and on empirical scaling relations, binary evolution in real galaxies was shown to take place in the "empty loss cone" (diffusive) regime for binaries with total mass above about $10^{5.5} M_\odot$. This regime is out of range of particle numbers currently feasible via direct N-body simulation but can be efficiently treated via the Fokker-Planck approximation.

4. Accurate analytical expressions were derived that reproduce the predictions of the Fokker-Planck model for the time-dependence of binary semi-major axis (equation 39) and the time to coalescence (equation 55) in the diffusive regime.

5. Based on the Fokker-Planck integrations and on empirical scaling relations, gravitational-radiation coalescence will occur in 10 Gyr or less for galaxies with binary masses $\lesssim 2 \times 10^6 M_\odot$ or central velocity dispersions $\lesssim 80$ km s^{-1}; the coalescence time depends only weakly on binary mass ratio (Fig. 19). Binaries with masses $\gtrsim 10^7 M_\odot$ will remain stalled for a Hubble time.

6. A core, or "mass deficit," is created as a result of competition between ejection of stars by the binary and re-supply of depleted orbits via gravitational (star-star) encounters. Mass deficits as large as $\sim 4(M_1 + M_2)$ were found to be generated before coalescence (Fig. 16,17).

7. After the black holes coalesce, a Bahcall-Wolf cusp forms around the single hole in approximately one relaxation time, resulting in a nuclear density profile with a flat core and an inner, compact cluster (Fig. 21), similar to what is observed at the centers of low-luminosity spheroids.

REFERENCES

Aarseth, S. J. 1999, PASP, 111, 1333
Aarseth, S. J. 2003, Ap&SS, 285, 367
Baranov, A. S. 1984, Soviet Astronomy, 28, 642
Berczik, P., Merritt, D. & Spurzem, R. 2005, ApJ, 633, 680 (Paper II)
Chatterjee, P., Hernquist, L., & Loeb, A. 2003, ApJ, 592, 32
Cohn, H. 1980, ApJ, 242, 765
Cohn, H., & Kulsrud, R. M. 1978, ApJ, 226, 1087
Côté, P., et al. 2004, ApJS, 153, 223
Dehnen, W. 1993, MNRAS, 265, 250
Ebisuzaki, T., Makino, J., & Okumura, S. K. 1991, Nature, 354, 212
Ferrarese, L., et al. 2006, ApJ, 644, L21
Ferrarese, L., & Ford, H. 2005, Space Science Reviews, 116, 523
Fukushige, T., Makino, J., & Kawai, A. 2005, ArXiv Astrophysics e-prints, arXiv:astro-ph/0504407
Governato, F., Colpi, M., & Maraschi, L. 1994, MNRAS, 271, 317
Graham, A. W. 2004, ApJ, 613, L33
Harfst, S., Gualandris, A., Merritt, D., Spurzem, R., Portegies Zwart, S., & Berczik, P. 2006, ArXiv Astrophysics e-prints, arXiv:astro-ph/0608125
Heggie, D. C., & Mathieu, R. D. 1986, LNP Vol. 267: The Use of Supercomputers in Stellar Dynamics, 267, 233
Hemsendorf, M., Sigurdsson, S., & Spurzem, R. 2002, ApJ, 581, 1256

Hernquist, L., & Ostriker, J. P. 1992, ApJ, 386, 375
Hills, J. G. 1983, AJ, 88, 1269
Hopman, C., & Alexander, T. 2006, ApJ, 645, L133
Kandrup, H. E., Sideris, I. V., Terzić, B., & Bohn, C. L. 2003, ApJ, 597, 111
King, I. R. 1966, AJ, 71, 64
Kustaanheimo, P. & Stiefel, E. 1965, J. Reine Angew. Math. 218, 204
Lightman, A. P., & Shapiro, S. L. 1977, ApJ, 211, 244
Magorrian, J., & Tremaine, S. 1999, MNRAS, 309, 447
Makino, J., & Aarseth, S. J. 1992, PASJ, 44, 141
Makino, J., & Funato, Y. 2004, ApJ, 602, 93
Makino, J., Fukushige, T., Okumura, S. K., & Ebisuzaki, T. 1993, PASJ, 45, 303
Merritt, D. 2000, Dynamics of Galaxies: from the Early Universe to the Present, 197, 221
Merritt, D. 2001, ApJ, 556, 245
Merritt, D. 2004, Physical Review Letters, 92, 201304
Merritt, D. 2006a, ApJ, 648, 976
Merritt, D., Harfst, S., & Bertone, G. 2007, Phys. Rev. D, 75, 043517
Merritt, D. & Szell, A. 2006, ApJ, 648, 890
Merritt, D., & Ferrarese, L. 2001, MNRAS, 320, L30
Merritt, D., & Milosavljević, M. 2005, Living Reviews in Relativity, 8, 8

Merritt, D., & Poon, M. Y. 2004, ApJ, 606,

Merritt, D., & Wang, J. 2005, ApJ, 621, L101

Mikkola, S., & Aarseth, S. J. 1990, Celestial Mechanics and Dynamical Astronomy, 47, 375

Mikkola, S., & Aarseth, S. J. 1993, Celestial Mechanics and Dynamical Astronomy, 57, 439

Mikkola, S., & Valtonen, M. J. 1992, MNRAS, 259, 115

Milosavljević, M., & Merritt, D. 2001, ApJ, 563, 34

Milosavljević, M., & Merritt, D. 2003, ApJ, 596, 860 (Paper I)

Milosavljević, M., Merritt, D., Rest, A., & van den Bosch, F. C. 2002, MNRAS, 331, L51

Murphy, B. W., Cohn, H. N., & Durisen, R. H. 1991, ApJ, 370, 60

Nakano, T. & Makino, J. 1999, ApJ, 510, 155

Peters, P. C. 1964, Physical Review , 136, 1224

Plummer, H. C. 1911, MNRAS, 71, 460

Quinlan, G. D. 1996a, New Astronomy, 1, 35

Quinlan, G. D. 1996b, New Astronomy, 1, 255

Quinlan, G. D. & Hernquist, L. 1997, New Astronomy, 2, 533

Rajagopal, M., & Romani, R. W. 1995, ApJ, 446, 543

Ravindranath, S., Ho, L. C., & Filippenko, A. V. 2002, ApJ, 566, 801

Rossa, J., van der Marel, R. P., Böker, T., Gerssen, J., Ho, L. C., Rix, H.-W., Shields, J. C., & Walcher, C.-J. 2006, AJ, 132, 1074

Saslaw, W. C., Valtonen, M. J., & Aarseth, S. J. 1974, ApJ, 190, 253

Sesana, A., Haardt, F., & Madau, P. 2007, ApJ, 660, 546

Spitzer, L. 1987, Dynamical Evolution of Globular Clusters (Princeton: Princeton University Press)

Thorne, K. S., & Braginskii, V. B. 1976, ApJ, 204, L1

Valtonen, M. J. 1996, Comments on Astrophysics, 18, 191

Vicari, A., Capuzzo-Dolcetta, R., & Merritt, D. 2006, ArXiv Astrophysics e-prints, arXiv:astro-ph/0612073

Volonteri, M., Haardt, F., & Madau, P. 2003a, ApJ, 582, 559

Volonteri, M., Madau, P., & Haardt, F. 2003b, ApJ, 593, 661

Volonteri, M., Madau, P., Quataert, E., & Rees, M. J. 2005, ApJ, 620, 69

Wehner, E. H., & Harris, W. E. 2006, ApJ, 644, L17

Yu, Q. 2002, MNRAS, 331, 935

Zier, C. 2006, ArXiv Astrophysics e-prints, arXiv:astro-ph/0610457

Zier, C. 2006, MNRAS, 371, L36

Zier, C., & Biermann, P. L. 2001, A&A, 377, 23